TRANSPORTATION RESEARCH BOARD
NATIONAL RESEARCH COUNCIL

IDEA

Innovations Deserving Exploratory Analysis Project

NATIONAL COOPERATIVE HIGHWAY RESEARCH PROGRAM

Report of Investigation

IDEA PROGRAM FINAL REPORT

Contract NCHRP-44

IDEA Program
Transportation Research Board
National Research Council

May 1999

Roller Mountable Asphalt Pavement Quality Indicator

Prepared by:
Edward J. Jaselskis and Hsiu C. Han
Iowa State University
Ames, IA

INNOVATIONS DESERVING EXPLORATORY ANALYSIS (IDEA) PROGRAMS
MANAGED BY THE TRANSPORTATION RESEARCH BOARD (TRB)

This NCHRP-IDEA investigation was completed as part of the National Cooperative Highway Research Program (NCHRP). The NCHRP-IDEA program is one of the four IDEA programs managed by the Transportation Research Board (TRB) to foster innovations in highway and intermodal surface transportation systems. The other three IDEA program areas are Transit-IDEA, which focuses on products and results for transit practice, in support of the Transit Cooperative Research Program (TCRP), Safety-IDEA, which focuses on motor carrier safety practice, in support of the Federal Motor Carrier Safety Administration and Federal Railroad Administration, and High Speed Rail-IDEA (HSR), which focuses on products and results for high speed rail practice, in support of the Federal Railroad Administration. The four IDEA program areas are integrated to promote the development and testing of nontraditional and innovative concepts, methods, and technologies for surface transportation systems.

For information on the IDEA Program contact IDEA Program, Transportation Research Board, 500 5th Street, N.W., Washington, D.C. 20001 (phone: 202/334-1461, fax: 202/334-3471, http://www.nationalacademies.org/trb/idea)

CONTENTS

CONTENTS (continued)

LIST OF FIGURES

LIST OF FIGURES (continued)

LIST OF TABLES

EXECUTIVE SUMMARY

In-place density of compacted asphalt mixes have traditionally been used as an indication of roadway pavement quality. These density measurements, however, have not been available in real time to make in-process corrections to the paving operation because the existing techniques require on the order of minutes (nuclear density gauge) to hours (core samples) to produce accurate density measurements. This project uses an approach to measure, for the first time, the density of asphalt mixes in real time using a differential microwave signal approach. Two antennas, one in front of a roller and the other behind it, will measure reflected microwave signals from the asphalt pavement and the change in signal characteristics will indicate to the operator the optimal compaction and density of the pavement. This technique may minimize the need to quantify the hot mix asphalt properties that change during the compaction process. Preliminary field studies demonstrated a relationship between asphalt pavement density and microwave signal variance.

This report summarizes work on the Roller Mountable Asphalt Pavement Quality Indicator project (NCHRP-44) funded by the Transportation Research Board IDEA Program. This will be referred to as the Microwave Asphalt Density Sensor (MADS) project in this report. The methodology involved first developing a better understanding of the electrodynamical properties of asphalt pavement using microwaves. Laboratory experimentation was performed at Vilnius University (VU) and Iowa State University. Vilnius University was provided with several small asphalt pavement samples consisting of two binder concentrations and two aggregate types. Significant findings from the work performed by VU related to measuring the dielectric parameters of asphalt in the frequency range from 100 Hz to 12 GHz and in the temperature range from 290 K to 450 K reveal the following results:

(1) Permittivity (ε') and losses (ε'') depend on frequency and temperature. However, at microwave frequencies 8 GHz to 12 GHz permittivity and loses are almost frequency independent.
(2) The permittivity and losses are proportional to the density of the asphalt.
(3) The absolute values of permittivity and losses were found in the large frequency and temperature range for the samples of different composition and density.
(4) Permittivity slightly increases with temperature.
(5) Moisture strongly increases permittivity and losses at low frequencies and only slightly at microwave frequencies.
(6) With 8 GHz and higher microwave frequencies, permittivity and losses are caused mainly by fundamental mechanisms of electronic and ionic polarization. Therefore, these values are parameters of the material but not sample composition and size.
(7) The penetration depth of microwaves in asphalt pavement is about 12 cm to 14 cm at 8 GHz and only 4 cm at 30 GHz.
(8) To control density of asphalt layers, the microwave frequency should be selected so that the penetration depth of microwaves should be smaller than asphalt layer thickness.

Iowa State University analyzed full-size samples provided by the Iowa Department of Transportation to further identify the source of the changing data variance as asphalt mix density changes. Experimental results show that the variance of microwave reflection decreases as asphalt mix density increases, but that near the point of optimum compaction, the variance of microwave reflection increases. These characteristics can be useful in developing a noncontact method for assessing the degree of compaction of asphalt pavement in real time.

From information obtained during the laboratory analysis, it was possible to design and build a prototype MADS system. Main components of the MADS system include the (1) microwave equipment, (2) supporting structure, (3) vibration isolation system, (4) signal sampling regulator, and (5) surface water removal system. Two field tests were conducted. The research team experienced some difficulties with both tests. In the first test, the outdoor temperature, roller vibration, and improperly calibrated sampling regulator compromised some of the results. In the second test, a tender mix design and an upward sloping mat caused the wheels on the carts to become stuck with binder and aggregate. Thus, the wheels needed periodic cleaning. Results from these tests were inconclusive since the decreasing variance trend discovered during the preliminary field tests could not be replicated. It appears that additional technical issues with the prototype need to be resolved and further tests conducted before this idea can be validated.

Based on the prototype results and those of the preliminary field tests, the principal investigators recommend continuing to refine the prototype differential microwave sensor. The future direction should involve more testing using a modified version of the original prototype. It would be ideal to eliminate the carts completely and use only one antenna mounted in the center of the roller. The differential approach can still work with one antenna as long as the roller operator compares signal variance from one coverage to another. As long as there is a decreasing variance trend, the operator would continue compacting that particular zone before moving to another part of the mat. It may also be necessary to change the microwave frequency to eliminate any possible subbase interaction. The principal investigators also recommend teaming with an industrial partner in the next phase. Some ideas have been discussed about how this could effectively be accomplished.

1. INTRODUCTION

Several teams are involved in the production of a quality asphalt pavement (e.g., design mix specifier, hot mix plant operator, asphalt laying operator, and roller compactor operator), but the roller operator's skill ultimately determines the final quality of the compacted mat. Since density measurement has been traditionally used as an indication of pavement quality, it can also serve as a measurement of the effectiveness of the compaction process. Other than the skill of the roller operator needed to produce a quality pavement, careful planning is needed to determine the rolling pattern that will produce the uniformity and desired density.

Improper compaction costs both the owner and the contractor. Owners receive a substandard pavement while contractors are penalized for improper compaction through a reduced payment. The pay scale for asphalt pavement contractors is based upon aggregate gradation, asphalt and mix properties, and in-place density; thus, improper compaction will result in a reduced payment. Another important consideration is the growing use of performance-based specifications. A performance-based specification states the required number of years that an asphalt pavement needs to last. This further reinforces the importance of obtaining the proper compaction level so the pavement will meet the specifications.

1.1 PROBLEM

Currently, several techniques determine asphalt pavement density. Core sampling is one common technique extensively used by departments of transportation for ensuring satisfactory specification compliance. Also, extensive effort has been devoted to nondestructive evaluation of asphalt density characteristics. Nuclear density gauges, for example, have been used for several years to measure the bulk density of hot asphalt mixtures. The capacitance energy dissipation method is another technique that is relatively new to the paving industry.

Each of the above techniques has its strengths and opportunities for enhancement. Coring is a destructive technique that ultimately weakens the pavement in places where samples are taken and provides density information too late for the paving contractor to make in-process corrections. The nuclear density gauge provides real-time density values but also requires (1) special handling and certification due to its radioactive contents, (2) proper calibration, and (3) surface contact for a certain period. The capacitance energy dissipation method is relatively new, and further work continues on developing its capabilities. Currently, this hand-held device requires calibration to a core of known density and involves momentary surface contact.

1.2 IDEA PRODUCT

The primary objective of this research is to develop an alternative asphalt pavement density sensing device that will provide real-time, in-process feedback to the roller operator regarding pavement density. Desirable characteristics include (1) roller mountable, (2) noncontact, (3) minimal health and safety concerns, and (4) minimal calibration (if any) for a given mix design.

1.3 CONCEPT AND INNOVATION

The new approach involves using microwave energy in a differential manner. Two antennas, one in front of a roller and the other behind it, measure reflected microwave signals from the asphalt pavement. A change in signal properties will show the operator the optimal compaction and density of the pavement (see Figure 1.1). Specific properties of the pavement such as binder chemistry and mat temperature are not factors since these properties are essentially the same in front and behind the roller. Preliminary field studies demonstrated the potential for implementing this idea. The results showed a decreasing trend in microwave signal variability as the density increased. In the area of optimal compaction (92 to 96% Rice density), signal variance significantly increased. A more detailed description of the preliminary field results can be found in the next chapter.

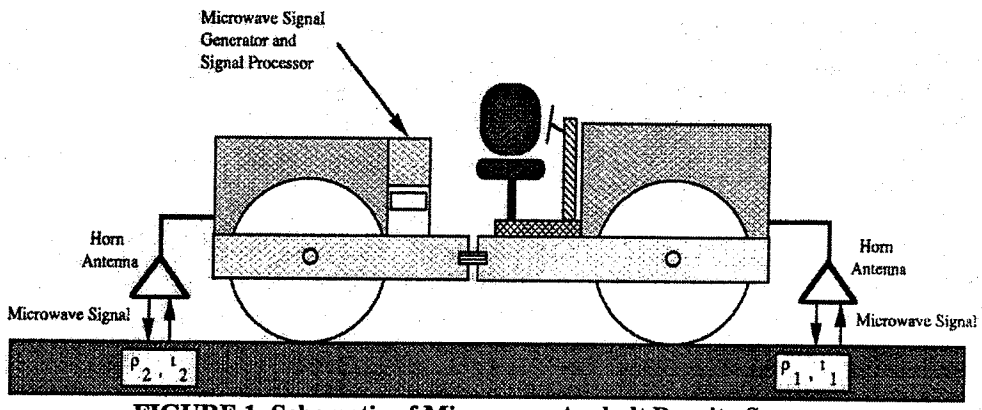

FIGURE 1 Schematic of Microwave Asphalt Density Sensor

Based on these findings, a new Microwave Asphalt Density Sensor (MADS) was developed. This sensor continuously provides the roller operator with real-time pavement density information. It is also noncontact, roller mountable, and safe. Furthermore, using the differential approach minimizes the need to quantify the hot mix asphalt (HMA) properties that change during the compaction process.

1.4 INVESTIGATION

The methodology for this research project involves three important steps: (1) performing extensive laboratory testing to determine the design parameters for developing a prototype, (2) designing and building a prototype system, and (3) field testing the prototype and analyzing the results. Iowa State University (ISU), the prime contractor, was supported in this effort by the Department of Radiophysics at Vilnius University (VU). Vilnius University exhibited a strong leadership role by providing extensive, rigorous laboratory testing of small asphalt pavement samples and solving important electrodynamical relationships. Iowa State University investigated the properties of full-size samples prepared by the Iowa Department of Transportation (IA DOT). Prototype development and field testing were exclusively performed at ISU.

1.5 REPORT ORGANIZATION

This report provides an informative description of the research and development involved in producing the first differential MADS. Preliminary field testing related to this idea is presented in Chapter 2. This chapter is significant since it provides some of the theoretical basis for this new density sensing approach. Chapter 3 describes the electrodynamical properties of asphalt pavement that were determined by extensive laboratory experiments and provides some of the theory behind this idea. All of this information is relevant to the successful development of the prototype. Chapter 4 describes the design and construction of the prototype. Chapter 5 describes the field test procedures and results using the new MADS. A summary, recommendations for future work, and conclusions are found in Chapter 6.

2.0 PRELIMINARY FIELD INVESTIGATION

This research is based on results obtained during two previous field tests that demonstrated a statistical relationship between signal variability and density. This chapter briefly describes those field test procedures and results.

2.1 OVERVIEW

Two field experiments were conducted prior to the start of this NCHRP-IDEA project to investigate microwave signal characteristics on asphalt pavement. The testing involved introducing microwave energy into asphalt pavement to investigate possible relationships between the return signal and pavement density.

2.2 FIELD SETUP AND PROCEDURES

In each field experiment, six asphalt strips, 8 feet wide and 25 feet long, were compacted to different levels using a vibratory roller. Microwave reflections from the asphalt surface were measured at 40 different points along each strip at 2-cm intervals. The data acquisition was performed with an HP 8410 network analyzer, an HP 8350B sweep oscillator, an X-band standard-gain horn antenna, and a computer-controlled linear antenna positioner. Figure 2.1 is a photograph of the field setup. Note that only one antenna was used during the preliminary field tests. The differential concept was simulated by comparing microwave signal values from one pavement density to another.

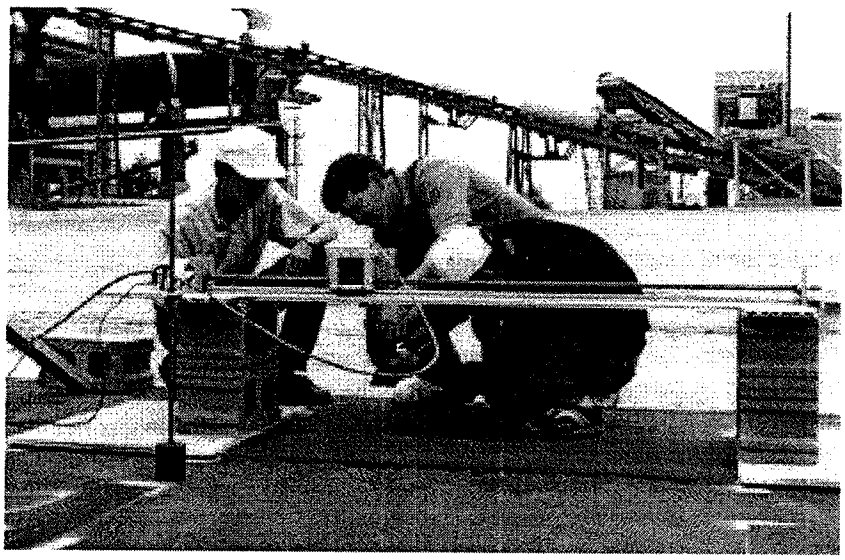

FIGURE 2.1 Photograph of Field Setup

Measurements were taken immediately after the paving was completed and repeated twice at approximately two hours and one day after the paving operation, respectively. The asphalt surface temperatures during those three tests were above 200 F (referred to as "hot" test), around 120 F (referred to as "warm" test), and the same as the ambient air temperature (referred to as "cold" test).

In the first preliminary field test, 11 different microwave frequencies between 8 and 12 GHz with 0.4 GHz increments were used; in the second test, only 8 GHz microwaves were used. In the first field test, measurements were taken at three different antenna elevations for the cold and warm tests, but at one elevation for the hot tests. In the second test, one elevation was used for both the hot and warm tests, and three for the cold test. The antenna looking direction was kept in the zenith for all measurements.

Three core samples were extracted from each strip and analyzed in the laboratory to provide the true asphalt density of each strip. The specifics of the field test arrangements are summarized in Table 2.1. The pavement is considered properly compacted if the asphalt density is in the range of 93 to 94% of the Rice density. (The Marshall density also could have been used as the density measurement criterion but was not.)

2.3 DATA ANALYSIS

An exploratory data analysis technique was performed to identify possible correlations between reflected signal magnitude and phase.

TABLE 2.1 Summary of Preliminary Field Experiment Parameters

Test Number	Roller Coverages	CW Frequency (GHz)	Asphalt Temperature	Antenna Elevation[1] (cm)
One	2, 4, 6, 8, 10, and 12	8.0, 8.4, 8.8, 9.2, 9.6, 10.0, 10.4, 10.8, 11.2, 11.6, and 12.0	Hot	15
			Warm	10, 12.5, and 15
			Cold	10, 12.5, and 15
Two	2, 4, 6, 8, 10, and 12	8	Hot	17[2]
	–	–	Warm	17[2]
	–	–	Cold	16.9, 17.1, and 17.3

[1] Antenna elevation is the distance from the pavement surface to the antenna aperture.
[2] Each of these tests were repeated twice at this antenna elevation.

The signal variance revealed some interesting trends: signal variability distinctly decreased as pavement density increased (see variance equation below). The variance in the zone of optimal compaction also sharply increased. Figure 2.2 provides plots of data acquired during the first hot asphalt test. Each plot in this figure shows the average variance of the 40 reflection coefficients measured along each of the six strips as a function of the asphalt density in the corresponding strip. Statistical analysis demonstrated that the signal variability for the real and imaginary components is normally distributed and thus follow a Rayleigh distribution [1].

$$\sigma^2 = \sum_{n=1}^{N} | c_n - \bar{c} |^2 \Big/ (N-1)$$

A qualitative feature can be observed in the variance plots shown in Figure 2.2. Initially, the variance in microwave reflection data decreases as asphalt density increases. After the density reaches a certain level, however, the variance increases again. The minimum variance takes place at approximately 93% of Rice density. Variance plots for the other six datasets (i.e., data from the three warm tests and the three cold tests) show trends identical to those described above. A second field test conducted at a later date also confirmed these findings.

A confidence analysis was performed to establish that a variance obtained from one coverage is significantly different from the variance obtained from another coverage. Since the real and imaginary components are normally distributed making the resulting reflection coefficient Rayleigh distributed, confidence intervals can be computed for the

separate components, then combined to obtain the confidence intervals for the Rayleigh variance. This can be performed since the Rayleigh variance is equal to the sum of the normal variance of the real and imaginary parts.

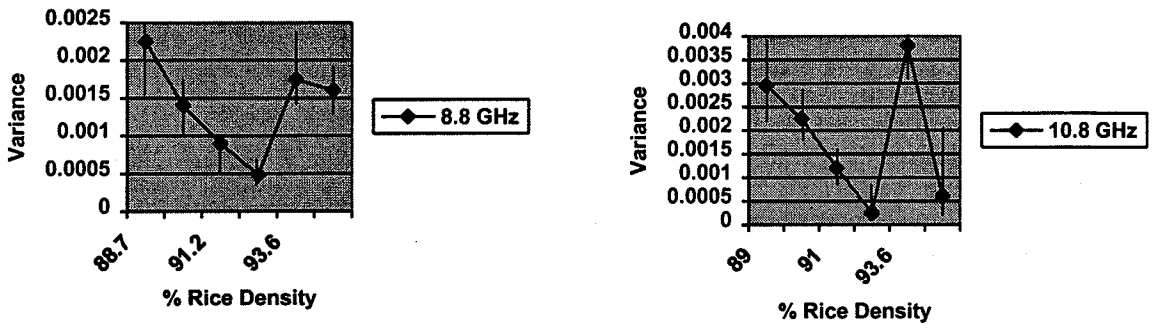

FIGURE 2.2 Variances from First Preliminary Field Test

Using this procedure, confidence limits are established for the data using an 80% confidence bound (refer to Figure 2.2). It can be seen that with only 40 points in the variance calculation, the possible error is the resulting variance can be relatively large. It is interesting to note that the confidence interval decreases as the density increases resulting in greater certainty that the optimal compaction level has been attained. For more information regarding these field tests, refer to Fahrion [1] and Han, et al. [2].

3.0 ELECTRODYNAMIC PROPERTIES OF ASPHALT PAVEMENT

Based on the encouraging findings of the preliminary field tests, the principal investigators (PIs) decided to continue this research project. The first step was to obtain a better understanding of the electrodynamical properties of asphalt pavement before developing a prototype microwave asphalt density sensor (MADS). To successfully accomplish this objective, a research team was established involving scientists at Vilnius University (VU) and Iowa State University (ISU). Vilnius University provided much of the expertise related to better understanding of the electrodynamical relations involved in this approach. Iowa State complemented VU's efforts by performing additional laboratory experiments and was principally responsible for designing, building, and testing the prototype.

This chapter discusses the electrodynamical properties of asphalt pavement. It begins with a description of the significant relationships that VU PIs knew were involved with using microwaves as an indicator of asphalt pavement density. The results from laboratory experiments conducted at VU and ISU are also included. Some of this information was used in the prototype design and development.

3.1 ELECTRODYNAMICAL RELATIONS

The amplitude and phase of the reflected microwave signal are functions of the complex permittivity of the asphalt mixture. In general, the complex permittivity, $\varepsilon^* = \varepsilon' - i\varepsilon''$, of a material affects how microwaves propagate and are attenuated in that material. In this case, the real part, ε', of the asphalt's complex permittivity is related to the pavement's polarization in the microwave field. It varies with the pavement composition, moisture content, and density. The imaginary part, ε'', describes the losses, i.e., the absorption and scattering of microwaves in the pavement.

The propagation constant of a plane microwave in asphalt is given by

$$\gamma^* = \gamma' - i\gamma'' = k_0\varepsilon^{*1/2} = (\omega^2\varepsilon_0\mu_0\varepsilon^*)^{1/2}, \tag{1}$$

where k_0 is the free space wavenumber that can be related to the microwave's wavelength, λ_0, through $k_0 = 2\pi/\lambda_0$; ω is the angular frequency of the microwave, ε_0; and μ_0 are the permittivity and permeability of free space, respectively, and

$$\gamma' = \omega\,(\varepsilon_0\mu_0\varepsilon')^{1/2}\,[1/2(1 + \tan^2\delta)^{1/2} + 1]^{1/2},$$
$$\gamma'' = \omega\,(\varepsilon_0\mu_0\varepsilon'')^{1/2}\,[1/2(1 + \tan^2\delta)^{1/2} - 1)^{1/2}.$$

The reflection coefficient for a microwave normally incident from free space on an infinite slab of asphalt whose thickness is d (see Figure 3.1 A) is given by

$$R = [R_i + R_j \exp(-2i\gamma d)] / [1 + R_iR_j \exp(-2i\gamma d)], \tag{2}$$

where

$$R_i = \{k_0 - \gamma\} / \{k_0 + \gamma\} = |R_i| \exp(I\varphi) \tag{3}$$

is the Fresnel reflection coefficient for the air-asphalt interface and R_j is the Fresnel reflection coefficient between the asphalt layer and the subbase. Thus, the reflection coefficient given by Equation (2) is a function of ε'; ε''; thickness of the mat, d; and frequency, ω, or wavelength, λ_0. The higher the microwave frequency, the shorter the penetration depth of microwaves.

Attenuation of microwaves is given by

$$L = \gamma''\, d\, 20 \log e \text{ [dB]}. \tag{4}$$

Absorption of microwaves can be calculated from the following equation:

$$P_{abs} = \varepsilon_0\, \varepsilon''\, \omega\, P_i \text{ [W/m]}, \tag{5}$$

where P_i is the incident power.

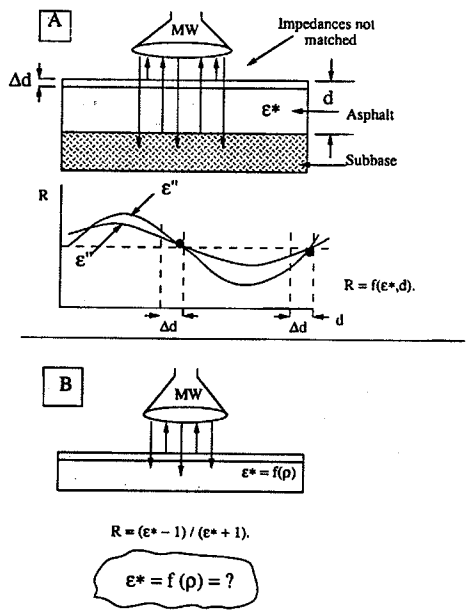

FIGURE 3.1 (A) Dependence of Reflected Signal Modulus on Thickness and ε"; (B) Reflected Signal Dependence on ε* or ρ

From Figure 3.1 A, it follows that when losses of the mat are not high, the reflected signal senses the asphalt and subbase (i.e., it depends on both the asphalt's complex permittivity and thickness). In this case, the reflected signal cannot be a measure of permittivity or density of asphalt layer only. During the compaction process, the reflectivity, R, may decrease or increase with decreasing thickness by the value Δd, depending on the value of the thickness, d. When the penetration depth of the microwave is smaller, it reflects only from the asphalt layer and does not penetrate the subbase, i.e., it depends only on permittivity or density, ρ, of the asphalt (see Figure 3.1 B). Thus, the penetration depth, as defined by the dielectric parameters of asphalt, is a very important parameter. That is why it is necessary to know (1) the dielectric parameters of asphalt and (2) how the complex permittivity, ε*, is related to asphalt density.

To experimentally find the direct relation between the reflection coefficient and the pavement density, it is necessary to use microwaves whose frequency does not penetrate through the entire asphalt layer. In this case, the reflection coefficient is independent of the asphalt layer thickness, d, and the reflection coefficient between the asphalt and the subbase. Thus, the amplitude of the reflected wave can be approximated by

$$R = (\varepsilon^* - 1) / (\varepsilon^* + 1). \tag{6}$$

The sensitivity of ε* to air voids or density of asphalt pavement causes the reflection coefficient to change. This change can be detected in the reflected signal and used to determine the asphalt pavement density.

3.2 VILNIUS UNIVERSITY LABORATORY RESULTS

In this section, the laboratory studies performed at VU are discussed; they include the following activities: (1) solve electrodynamic problems for precise microwave measurements of electrical parameters of asphalt for waveguide mode, (2) conduct laboratory experiments to determine waveguide reflection and transmission measurements of asphalt samples of different densities at various frequencies between 8 to 30 GHz and temperatures between 20 to 180°C (70 to 350°F), (3) calculate temperature and frequency dependencies of permittivity for asphalt samples of different density, (4) characterize and understand any observed deviations from theory, and (5) evaluate frequency band needed.

3.2.1 Procedures

Dielectric studies were performed on small samples provided by ISU in the 100 Hz to 12 GHz frequency range. In the 100 Hz to 1 MHz range, the computer-controlled LCR meter HP 4284A was used. In the 10 MHz to 4 GHz range, a

coaxial dielectric spectrometer setup was used. The sample ends were coated with silver paste and put into the sample holders. The sample holder was squeezed between the inner conductor of the coaxial and the short. The complex permittivity was calculated from the formula of the dynamical coaxial capacitor, taking into account the sample's inhomogeneous distribution of the electric field at microwave frequencies. The temperature dependencies were studied with the rate of 0.1 K/min on heating or cooling.

For higher frequencies, the waveguide technique was used. Vilnius University researchers had to solve the electrodynamical problem of defining the relation of the asphalt rod's dielectric parameters to the microwave's reflection and transmission coefficients. A large frequency range was used to understand which polarization mechanisms define dielectric parameters.

Detailed information regarding the setup procedures and solutions to electrodynamical problems can be found in the Appendixes. Appendix A provides the calculations necessary for determining the properties of a dielectric cylinder using a rectangular waveguide. Appendix B provides an explanation of how dielectric parameters are determined for each sample.

3.2.2 Experimental Results

Small asphalt samples were made using both sand ("S") and crushed rock ("R") as the aggregate. Each sample was cylindrically shaped (1 cm in diameter and approximately 1 cm in height). The sand samples included two different percentages of asphalt binder (8.4% and 4%). The rock samples also used two different percentages of asphalt binder (8.5% and 4%). Thus, there were four sample categories: (1) S 8.4, (2) S 4, (3) R 8.5, and (4) R 4. As Table 3.1 shows, three density ranges were provided for each of these categories.

TABLE 3.1 Small Sample Properties

Density Range (Lbs/Cubic Foot)	Sand w/8.4% Binder (S 8.4)	Sand w/4% Binder (S4)	Rock w/8.5% Binder (R 8.4)	Rock w/4% Binder (R 4)
High	140-150	140-145	140-150	140-150
Medium	130-140	120-130	120-130	Not Possible
Low	110-120	100-110	110-120	Not Possible

In each of the 12 possible categories, three samples were made. It was not possible to produce R 4 samples in the Medium and Low ranges because they were too brittle.

3.2.2.1 Frequency Dependence of Permittivity and Losses

Figure 3.2 shows the frequency dependence of permittivity (ε') of the S 8.4 samples of the three different densities in the 10^2 to 10^{10} Hz frequency range. With the increase of frequency, permittivity decreases and is slightly dependent on frequency at microwaves. In the 8 to 12 GHz frequency range, permittivity is almost independent of frequency. This result shows that below 10^8 Hz, asphalt's dielectric properties are caused not only by fundamental mechanisms of polarization (electronic, ionic, and dipole polarization) but also by interfacial polarization of inhomogeneous material. At about 8 GHz and higher frequencies, only electronic and ionic polarization defines the permittivity of asphalt. In this case, permittivity is a parameter of the material and not of a specific sample. In other words, the sample dimensions are not relevant since the permittivity is principally a property of the material. One can see that permittivity depends on sample density: the higher the density, the higher the permittivity. Measurement accuracy is also shown in the figure.

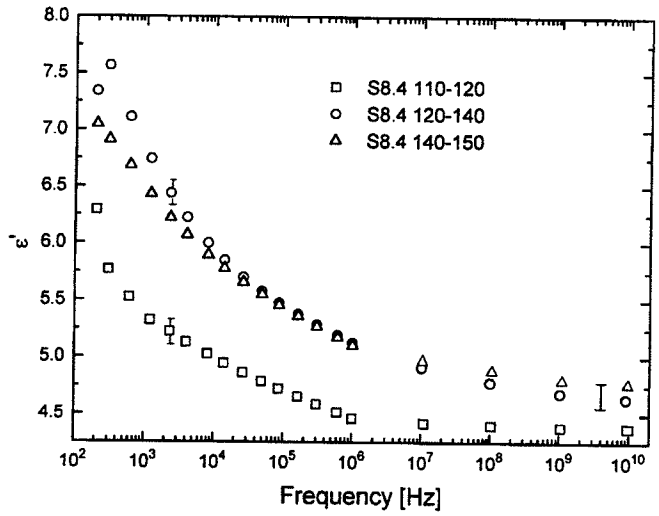

FIGURE 3.2 Frequency Dependence of Permittivity of the S 8.4 Asphalt Samples

Figure 3.3 shows the frequency dependence of the losses (ε") for the same S 8.4 samples. Losses are also strongly frequency dependent at low frequencies and almost independent of frequency at microwaves when interfacial polarization ends. Losses are less dependent on density of the samples than permittivity.

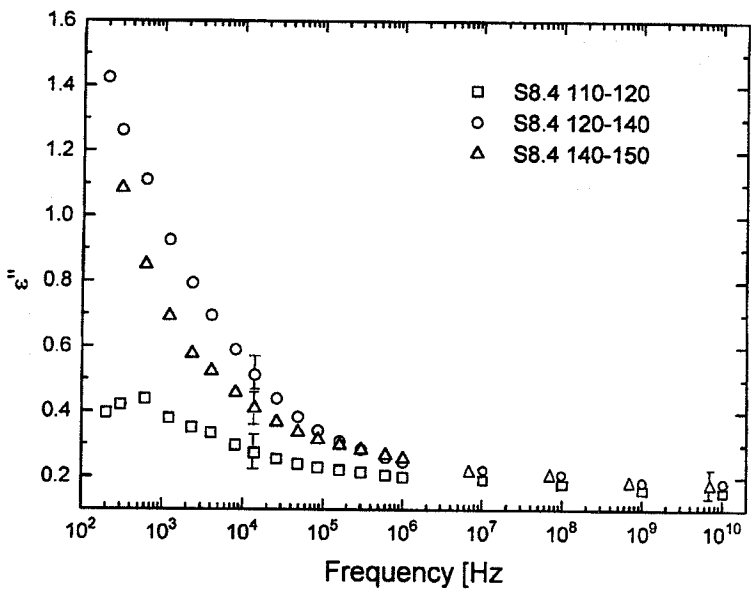

FIGURE 3.3 Frequency Dependence of Losses for the S 8.4 Asphalt Samples

Figure 3.4 shows the frequency dependence of permittivity of S 4 samples of two different densities, 100-110 and 120-130 lbs/ft^3 at frequencies below 1 MHz. A strong dependence of permittivity was observed on density in this frequency range. The same correlation was observed: the higher the density, the higher the permittivity. The research team heated one sample to 390 K and again measured frequency dependence of permittivity. The difference of permittivity of heated and nonheated samples is significant only at low frequencies. At microwaves, this difference is negligible.

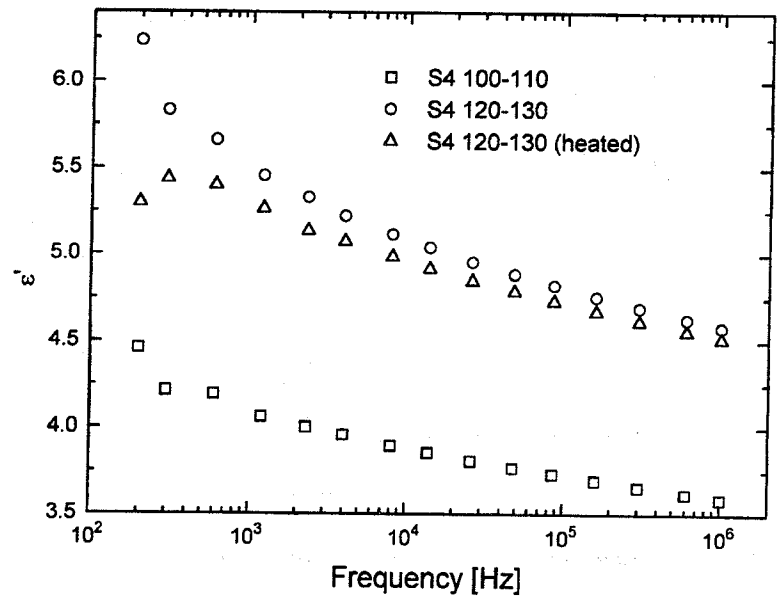

FIGURE 3.4 Frequency Dependence of Permittivity for the S 4 Asphalt Samples

Figure 3.5 shows frequency dependencies of the losses of the S 4 asphalt samples up to the frequency of 10 GHz. At microwaves, losses are similar as to those found in the previous sample and remain unchanged after heating the sample. However, losses are higher in the sample with higher density.

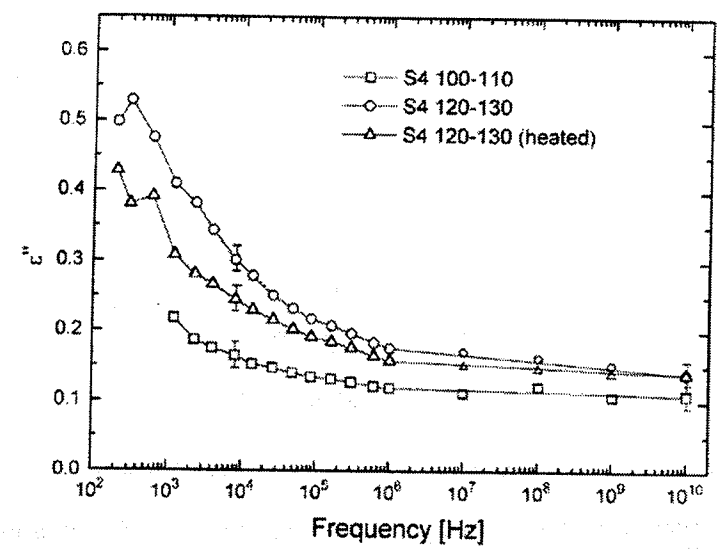

FIGURE 3.5 Frequency Dependence of Losses of the S 4 Asphalt Samples

Figure 3.6 shows the frequency dependence of the permittivity of the R 8.5 asphalt samples of three different densities. A clear correlation between permittivity and density of the samples at any frequency can be observed: the higher the density, the higher the permittivity of asphalt is. Accuracy of measurements is also indicated in the figure. Values of permittivity of R 8.5 samples are higher than of S 8.4 samples due to higher polarizability of rock matter. This result allows evaluation of what the sensitivity should be for the microwave asphalt pavement density sensor.

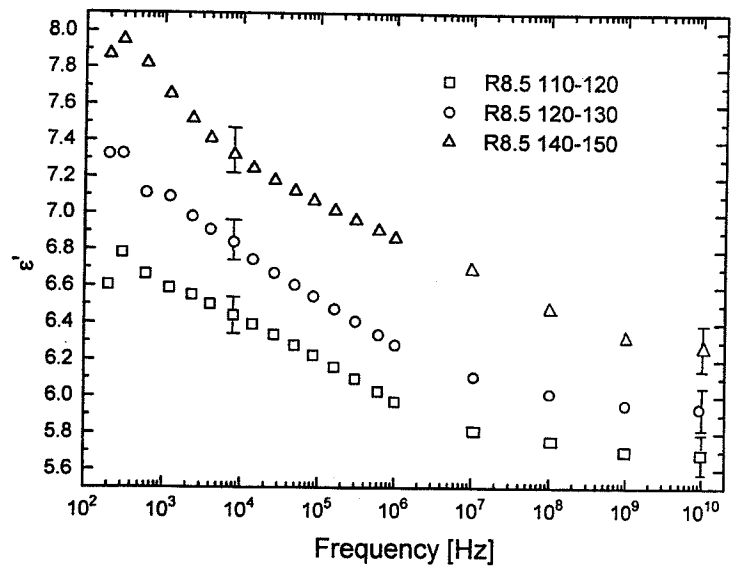

FIGURE 3.6 Frequency Dependence of Permittivity of the R 8.5 Asphalt Samples

Figure 3.7 shows frequency dependencies of the losses of the same R 8.5 asphalt samples. At microwaves, losses slightly depend on frequency and density of the samples.

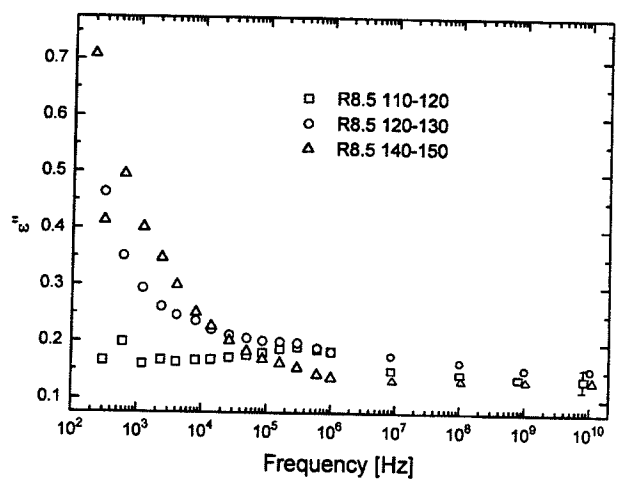

FIGURE 3.7 Frequency Dependence of Losses of the R 8.5 Asphalt Samples

Figure 3.8 shows the frequency dependence of the permittivity of the R 4 virgin asphalt sample and after heating it up to 390 K. After heating, the permittivity became slightly higher at all frequencies. Figure 3.9 shows a similar dependence of losses. This figure clearly indicates that losses are high only at low frequencies and are caused by conductivity of inhomogeneous asphalt matter. At high frequencies and microwaves, losses are small, mostly caused by the fundamental mechanism of ionic polarization and practically unchanged after the asphalt sample is heated.

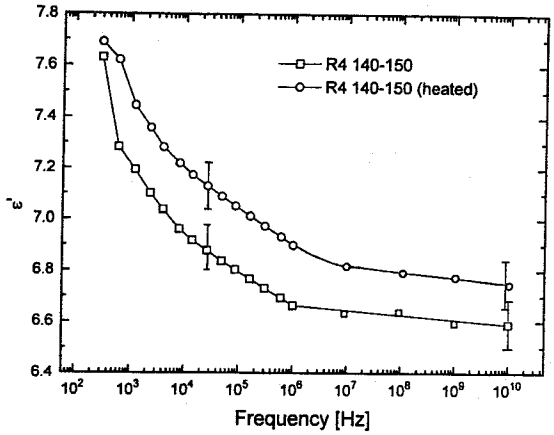

FIGURE 3.8 Frequency Dependence of Permittivity of the R 4 Asphalt Samples Before and After Heating

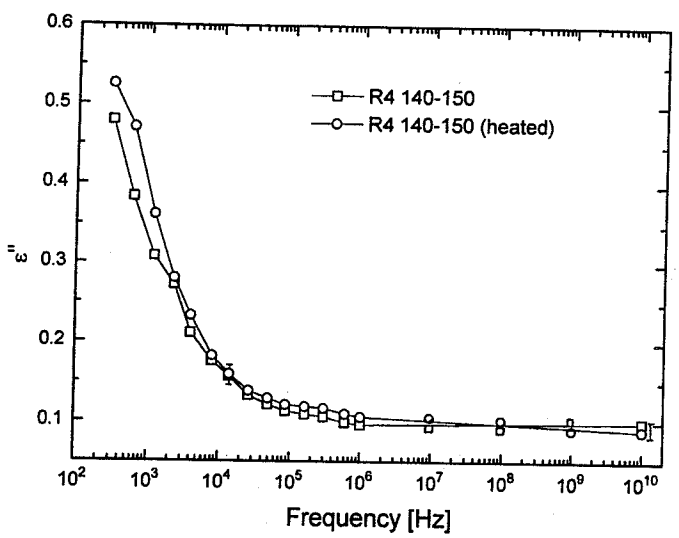

FIGURE 3.9 Frequency Dependence of Losses of the R 4 Asphalt Samples Before and After Heating

Thus, the measurements of complex permittivity of asphalt in the frequency range 100 Hz to 12 GHz have shown that:

(1) Permittivity and losses depend on frequency. This dependence at low frequencies is caused by interfacial polarization in inhomogeneous material. At frequencies between 8 and 12 GHz, both values are almost frequency independent; they are caused only by electronic and ionic mechanisms of polarization and are values of the material, not a specific sample.
(2) The higher the density, the higher are permittivity and losses.
(3) The absolute values of permittivity and losses at microwaves for different asphalt densities are as follows:

3.2.2.2 Temperature Dependence of Permittivity and Losses

R 8.5: $\varepsilon'(\rho) = 5.7$ to 6.3; $\varepsilon''(\rho) = 0.12$ to 0.16; $\tan\delta = 0.02$ to 0.03.

R 4: ε' (ρ) = 6.5 to 6.7; ε" (ρ) ≅ 0.1; tanδ ≅ 0.02.
S 8.4: ε'(ρ) = to 4.75; ε"(ρ) = 0.18 to 0.019; tanδ = 0.04.
S 4: ε'(ρ) = 3.8 to 4.4; ε" (ρ) = 0.12 to 0.14(0.3 to 0.4); tanδ ≅ 0.03 (0.09).

It is necessary to understand how dielectric parameters defining the microwave reflection depend on asphalt temperature. Figure 3.10 shows temperature dependence of permittivity and losses of the S 8.4 sample at a frequency of 1 MHz. If losses slightly depend on temperature, permittivity clearly has a maximum at about 375 K. This maximum of permittivity is related to the evaporation of water from the asphalt.

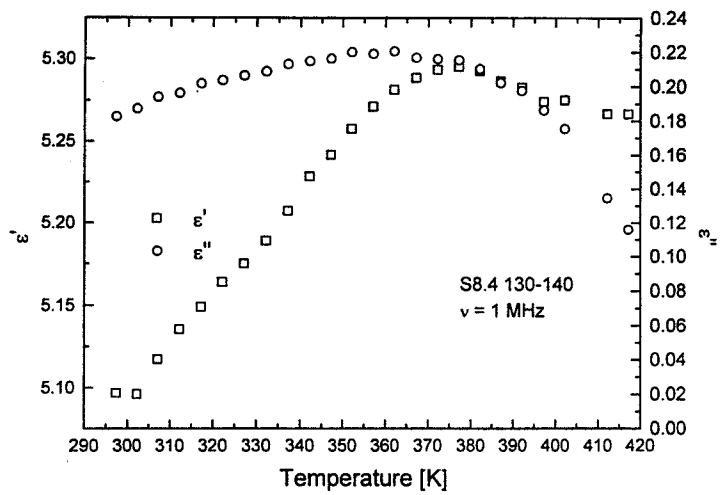

FIGURE 3.10 Temperature Dependence of ε' and ε" of the S 8.4 Asphalt Samples

Figure 3.11 shows the temperature dependence of ε' and ε" in the 140 to 150 lbs/ft^3 density range for the S 8.4 samples at the frequency 10 GHz. At this frequency, permittivity and losses only slightly depend on temperature. The maximum value of permittivity at 375 K is much smaller than at lower frequencies.

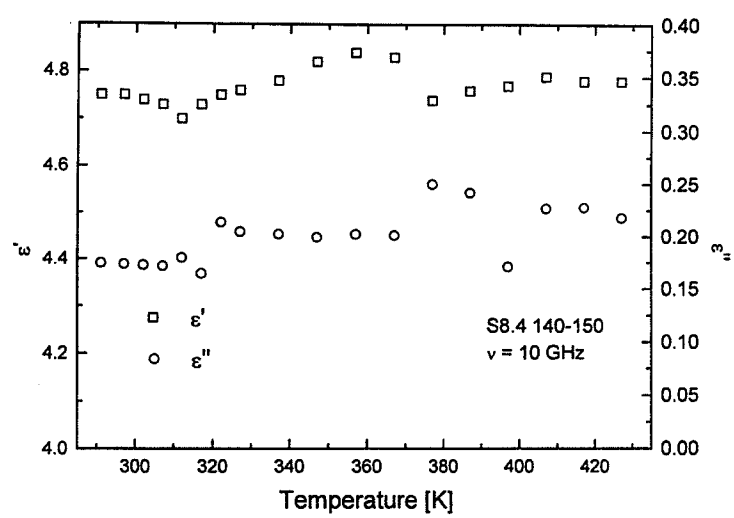

FIGURE 3.11 Permittivity and Losses vs. Temperature for the S 8.4 Asphalt Samples

Figures 3.12 and 3.13 show temperature dependencies of permittivity and losses of the S 4 samples of two different densities at microwave frequencies. The behavior of these parameters is different, but permittivity in both cases increases while losses fluctuate in the 0.3 to 0.4 range.

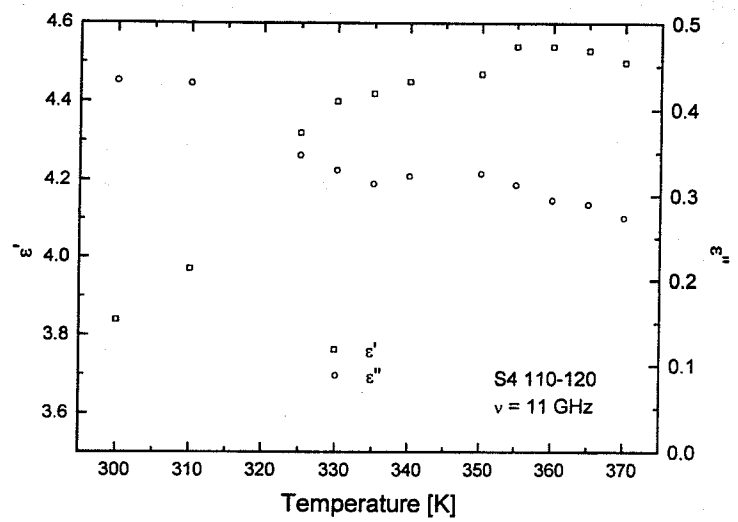

FIGURE 3.12 Temperature Dependence of Permittivity and Losses of the S 4 Asphalt Samples at 11 GHz

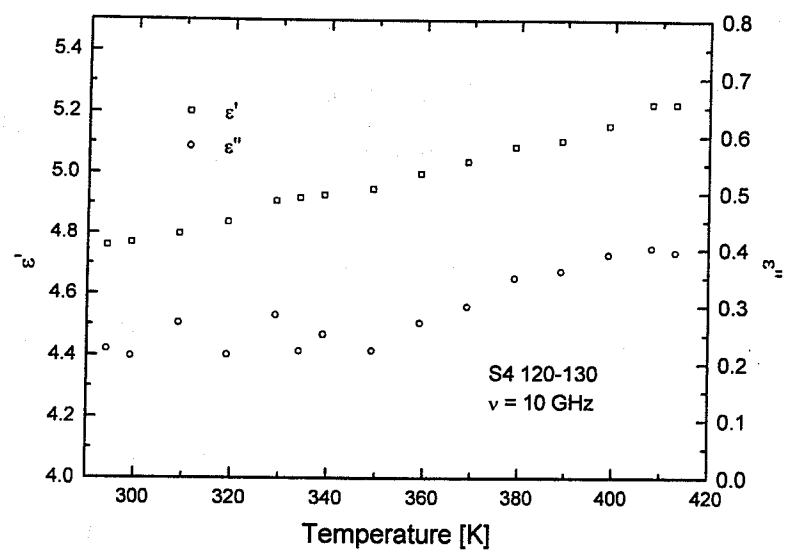

FIGURE 3.13 Temperature Dependence of Permittivity and Losses of the S 4 Asphalt Samples at 10 GHz

Figure 3.14 shows the temperature dependence of permittivity and losses of the R 4 asphalt sample at a frequency of 1 MHz. Permittivity increases with temperature while losses are almost constant.

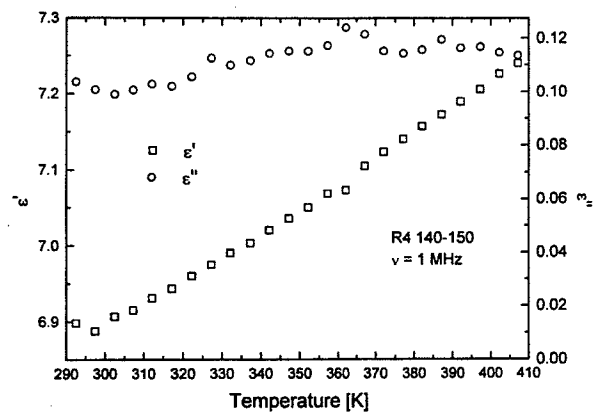

FIGURE 3.14 Temperature Dependence of Permittivity and Losses of R 4 Asphalt Samples

Figure 3.15 shows temperature dependence of permittivity and losses of the R 8.5 asphalt sample at frequency of 10 GHz. Within the accuracy of measurements, these values are almost independent of temperature.

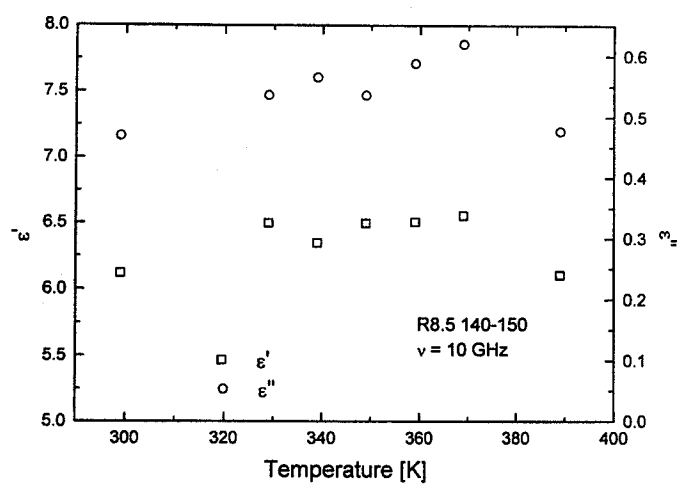

FIGURE 3.15 Temperature Dependence of Permittivity and Losses of R 8.5 Asphalt Samples

When a sample is heated up to 460 K, irreversible processes appear in the sample. Figure 3.16 shows an example of the temperature dependence of permittivity and losses of the R 8.5 asphalt sample of the density 140 to 150 lbs/ft^3 at a frequency of 1 MHz. Arrows show how the parameters change during the heating cycle: after heating, permittivity and losses decrease. This is related to changes in the organic microstructure of asphalt pavement.

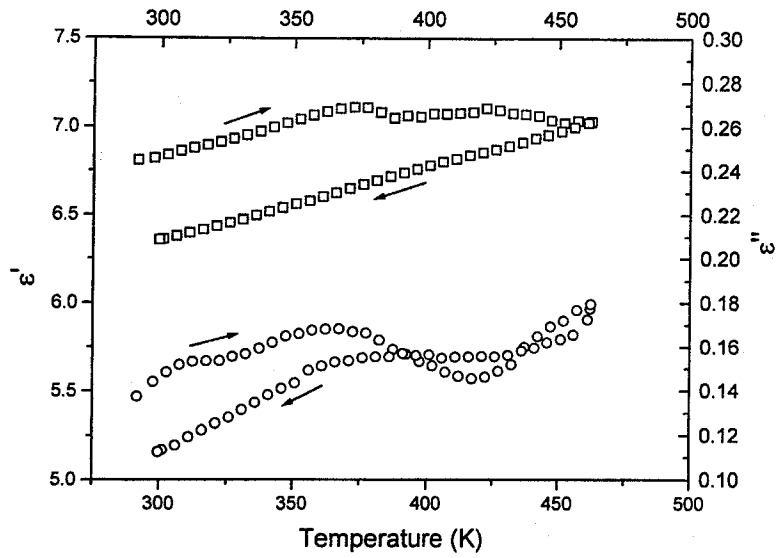

FIGURE 3.16 Cycle of Temperature Dependence of Permittivity and Losses of R 8.5 Asphalt Samples at 1 MHz

From the studies, it follows that permittivity of the asphalt samples at microwaves only slightly increases with temperature. After heating to 460 K or higher, the dielectric parameters of asphalt change irreversibly.

3.2.2.3 Permittivity and Losses of Wet Samples

The VU research team found that moisture strongly increases dielectric parameters of asphalt samples at low frequencies. Figure 3.17 shows frequency dependence of permittivity and losses of the R 8.5 sample.

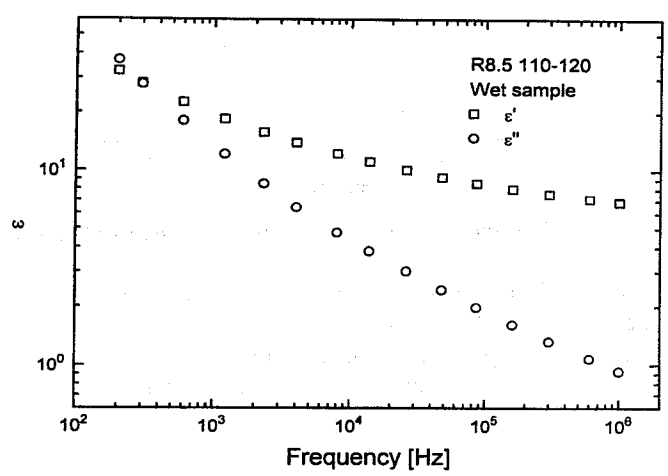

FIGURE 3.17 Frequency Dependence of ε' and ε" of Wet R 8.5 Asphalt Samples

Figures 3.18 and 3.19 show frequency dependencies of permittivity and losses of wet S 8.4 samples of different densities. It was determined found that moisture increases both dielectric parameters at low frequencies by several orders of magnitude. However, at or above the MHz region, these parameters approach the normal value of the dry samples.

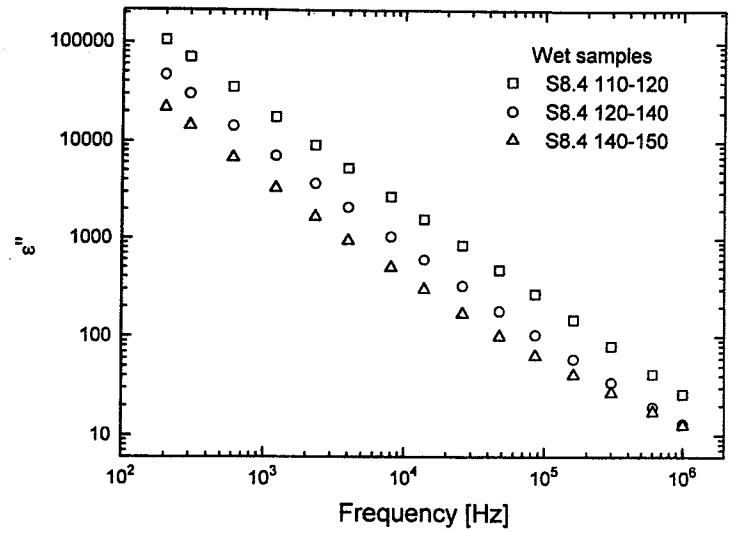

FIGURE 3.18 Frequency Dependence of Permittivity of Wet S 8.4 Asphalt Samples

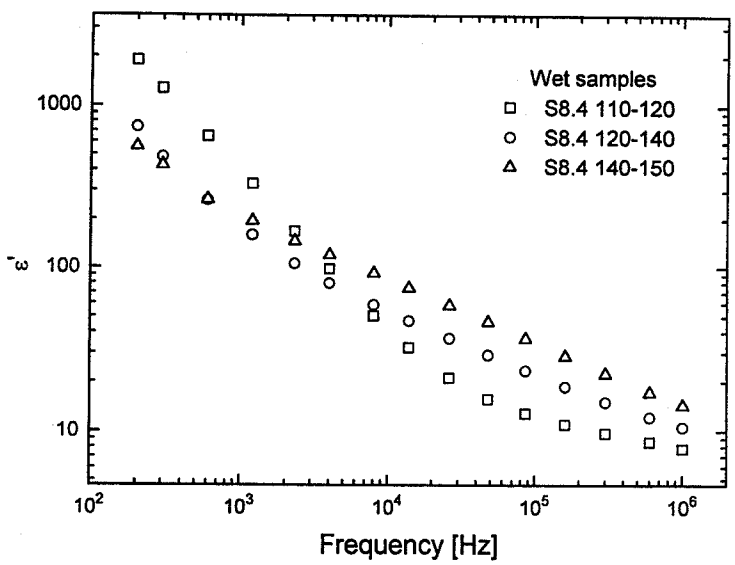

FIGURE 3.19 Frequency Dependence of Losses of Wet S 8.4 Asphalt Samples

The following conclusions can be drawn from the above experimentation: (1) the higher the density of asphalt, the less the moisture influences dielectric parameters and (2) moisture mostly influences dielectric parameters at low frequencies and very little at microwave frequencies.

3.2.2.4 Attenuation and Penetration Depth of Microwaves in Asphalt

With the dielectric parameters presented above and using Equation (4), the attenuation and penetration depth of microwaves in asphalt pavement were calculated. Figure 3.20 shows an example of the frequency dependence of the

attenuation of microwaves in asphalt pavement with the characteristic dielectric parameters ε' = 6.2 and ε" = 0.2 for four different layer thickness, d = 10; 15; 20; and 30 cm. With the increase of frequency, attenuation of microwaves in an asphalt layer increases. When the frequency of microwaves is 10 GHz, the layer of d = 10 cm attenuates only about 7 dB. The lower the attenuation, the deeper the microwaves penetrate. Clearly, microwaves of such frequency will penetrate deeply and reflect also from a subbase (see Figure 3.1 A). Thus, higher frequencies should be used for thin asphalt pavement layers.

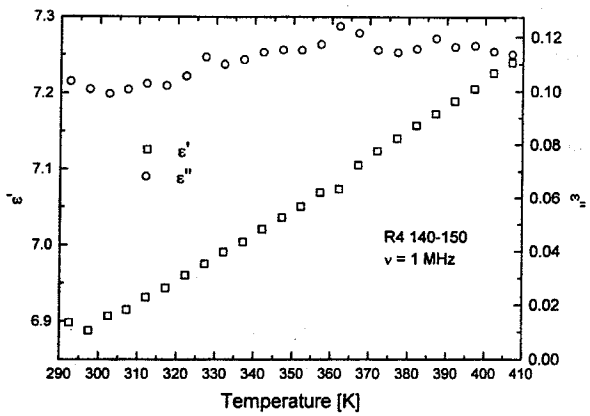

FIGURE 3.20 Frequency Dependence of Attenuation of Microwaves in Asphalt Pavement

Figure 3.21 shows the penetration depth of microwaves in asphalt pavement as a function of frequency with the characteristic dielectric parameters. Microwaves of 10-GHz frequency penetrate to approximately 12 cm in asphalt pavement, while microwaves of 30 GHz penetrate only to 4 cm. The results presented in this figure enable a proper microwave frequency to be selected that probes asphalt pavement. Only when microwaves reflect from the asphalt pavement, but not from the subbase (see Figure 3.1 B), can one relate reflected signal with permittivity or density of the asphalt pavement.

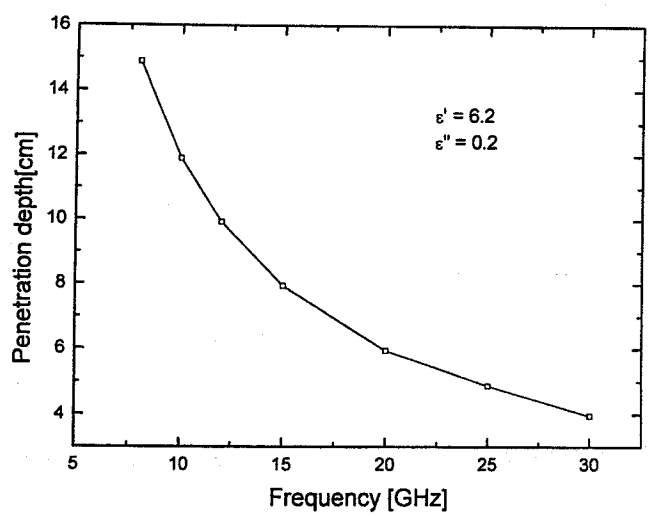

FIGURE 3.21 Frequency Dependence of Penetration Depth of Microwaves in Asphalt Pavement

3.2.2.5 Summary and Conclusions

Measurements of dielectric parameters of asphalt in the 100 Hz to 12 GHz frequency range and in the 290 to 450 K temperature range have shown that:

(1) Permittivity (ε') and losses (ε") depend on frequency and temperature. However, at 8 to 12 GHz microwave frequencies, permittivity and losses are nearly frequency independent.
(2) The higher the density of the asphalt, the higher the permittivity and losses.
(3) The absolute values of permittivity and losses were found in the large frequency and temperature range for the samples of different composition and density.
(4) Permittivity slightly increases with temperature.
(5) Moisture strongly increases permittivity and losses at low frequencies and only slightly at microwaves.
(6) At 8 GHz and higher microwave frequencies, permittivity and loses are caused mainly by fundamental mechanisms of electronic and ionic polarization. Therefore, these values are parameters of material and not a specific sample.

The penetration depth of microwaves in asphalt pavement is about 12 to 14 cm at 8 GHz and only 4 cm at 30 GHz. To control the density of asphalt layers, the microwave frequency should be selected so that the penetration depth of microwaves is smaller than asphalt layer thickness.

3.3 IOWA STATE UNIVERSITY LABORATORY RESULTS

The purpose of laboratory tests at ISU was to investigate microwave interaction on full-size samples of asphalt pavement. Using a gyratory compactor, 120 cylindrical asphalt samples were made at the IaDOT pavement research laboratory. All 120 samples had the same diameter of 150 mm and were divided into 6 density groups that each had 20 samples. The densities of the six density groups and the corresponding sample heights are listed in Table 3.2. The maximum specific gravity of the asphalt mix used in the laboratory samples is 2.455. The densities increased from 88% to 98% of Rice density in 2% increments.

TABLE 3.2 Large Sample Properties

% Maximum Specific Gravity	88.07	89.67	91.83	93.77	96.06	98.00
Sample Height (mm)	130	127	123	120	117	114

Using microwaves, the ISU research team investigated the bulk scattering properties of these samples. The experiment required the team to set each sample on a metal plate and measure the reflection coefficient using microwaves. The mean and variance of the reflection coefficients were determined for each density. Due to a shortage of time, however, tests involving surface roughness and moisture were not performed.

The samples were placed over a large aluminum plate, and microwave reflection coefficient at 8 GHz was measured for each sample with an open-ended waveguide in direct contact with the top surface of the sample. The variance of the reflection coefficients from the 20 samples in each density group was then calculated. Results lead to a consistent overall picture of how data variance changes as a function of asphalt density. In general terms, the data variance decreases as density increases beyond approximately 89 to 90% of the Rice density and reaches a minimum near approximately 93% of the Rice density; then data variance increases as density increases further.

The ISU study demonstrated that there is potential to use the variance of microwave reflection to determine asphalt pavement density. Experimental results show that the variance of microwave reflection decreases as asphalt density increases, but that near the point of optimum compaction, the variance of microwave reflection increases. This characteristic can be useful in developing a non-contact method for assessing the degree of compaction of asphalt pavement in real time.

4.0 PROTOTYPE CONCEPT AND DEVELOPMENT

This chapter provides a general description of the prototype concept as well as a detailed discussion of prototype development. The basis for prototype development was some of the findings from the preliminary field and laboratory investigations performed at VU and ISU. Much of the material from this chapter comes from a master's thesis reporting on the project [3].

4.1 PROTOTYPE CONCEPT

The Microwave Asphalt Density Sensor (MADS) operates by simultaneously comparing reflected microwave signals from the front and the rear of a vibratory roller. Two horn antennas continuously transmit microwaves into the asphalt, while a signal regulator triggers a computer, obtaining reflected signals at a regular interval. These signals are continuously processed during the vibratory roller operation. The computer calculates the variability of the signals, and the results are immediately available. Before compaction, the pavement is less dense, and the reflected signals exhibit higher variability (based on preliminary field studies). A significant rise in signal variability occurs when the pavement has reached its optimal level of compaction.

4.2 PROTOTYPE DEVELOPMENT

A prototype was built to validate the differential theory based on the requirements of the original concept. As discussed in the next section, a list of design criteria was initially developed.

Some of the long-lead items such as the microwave sources required a three- to four-month order and shipment time period. Due to the fast-track nature of this project, however, it was necessary to make decisions based on the most current information. The ISU research team decided to retain several design parameters that were used during the preliminary field tests. These parameters involved using an 8.5 GHz system and raising the antennas 15 cm from the pavement. If the pertinent VU findings had been available earlier, the ISU research team might have elected to use a higher microwave frequency.

4.2.1 Design Requirements

Several design criteria were addressed that assisted in developing the final design concept. The intent was to design the prototype such that the sensor would be roller mountable, operate in a noncontact mode, require minimal (if any) calibration for a given mix design, and would be safe.

One of the design considerations the team addressed was the vibration from the vibratory roller. Two types of vibration are present during the compaction process using a breakdown roller: ground vibration and transmitted vibration from the roller. Both types of vibration had to be addressed in the design because the microwave horn antennas are sensitive to changes in height and vibrations. In addition, the computer also had to be isolated from vibration to prevent damage.

Water was also a consideration during the design phase. During the compaction process, water is sprayed on the roller drums to prevent the hot asphalt from sticking to the drums. Puddles of water sometimes form on the asphalt surface that can detrimentally impact the reflected microwave signals. In a field study, the ISU research team found that water tends to increase the signal variance. Another consideration related to maintaining a constant antenna height to the pavement (15 cm was selected based on preliminary field test results). Variability of the microwave signals is quite sensitive to changes in antenna height.

After 3 to 4 months of deliberation on various design concepts, the ISU research team eventually decided on the final design format, which is discussed in the next section.

4.2.2 Final Design

Figure 4.1 shows an overall schematic of the final design. Carts were used to support the antennas located in the front and rear of the roller because they made it easier to maintain a constant height during the rolling operation. Each cart rolls on four high-temperature caster wheels capable of withstanding the heat from the hot asphalt. The cart, which has a

vibration isolation system to protect the equipment, supports the microwave equipment and the antenna. A signal sampling regulator, which pulses the computer to take measurements at discrete intervals, is also a key part of the design.

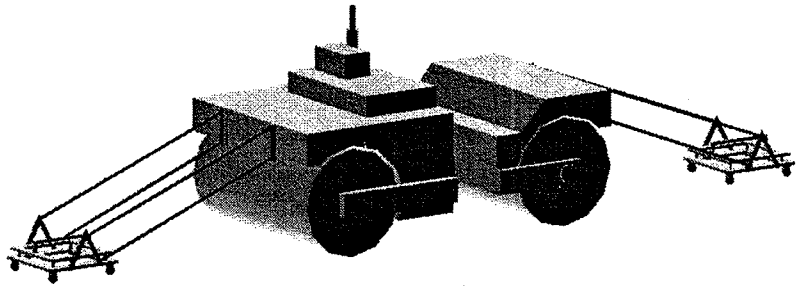

FIGURE 4.1 Final Design Concept

This final prototype design was broken into the following components that are discussed further in this report:

- Microwave equipment
- Supporting structure
- Vibration dampening system
- Signal sampling regulator
- Surface water removal system

4.2.2.1 Microwave Equipment

The microwave equipment used in the MADS comprise two coherent low-powered microwave sources producing microwaves at a fixed frequency. The signals are fed into a directional coupler that sends the signal to the circulator, which then sends a reference signal to the mixer. From the circulator, the signal is directed to the microwave antenna, which is directed perpendicular to the pavement. The reflected microwave signals are collected by the antenna and fed back into the mixer through the circulator. The mixer compares the reference and the reflected signals and then sends a signal comprising a real and imaginary part to the analog-to-digital (A/D) converter. These signals are converted into a digital format and processed by a computer. See Figure 4.2 for the design schematic.

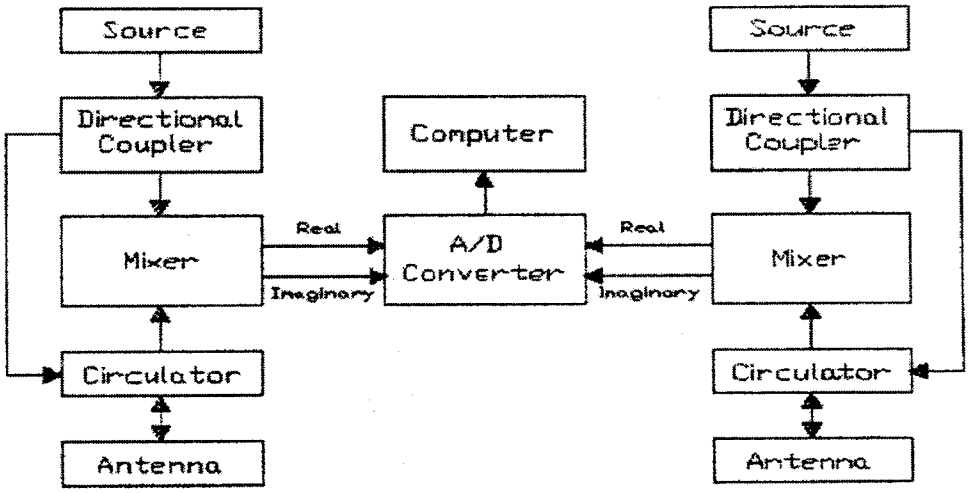

FIGURE 4.2 Microwave Design Schematic

A list of the microwave equipment and specifications is as follows:

Mixer

- Manufacturer: Anaren
- Model: 250128
- Quadrature IF mixer operating at 8 to 12.4 GHz

Microwave Source

- Manufacturer: Narda
- Model: NHO-XF-8500
- Output frequency: 8.5 GHz

Directional Coupler

- Manufacturer: M/A Com
- Model: 2020-6620-06
- Operating frequency: 8 to 12 GHz

Circulator

- Manufacturer: Narda
- Model: 4925
- Operating frequency: 8 to 12 GHz

Adapter

- Manufacturer: M/A Com
- Model: 2000-6254-00
- Operating frequency: 8.2 to 12.4 GHz
- Converts coaxial connections to antenna waveguide opening

Horn Antenna

- Manufacturer: Narda
- Model: 640
- Operating frequency: 8.2 to 12.4 GHz

Most of the microwave equipment was assembled into an aluminum box that was placed on the upper platform of the carts. The equipment placed in the box included the mixer, source, directional coupler, circulator, op-amp, and cooling fan. The microwave horn antenna was then attached to the bottom of the aluminum casing. The microwave box was fabricated with a quick-release design. Two vertical rods and pins held the box in place. By removing the pins, the height of the box could be adjusted or the box could be completely removed. The internal layout of the completed microwave box is shown in Figure 4.3.

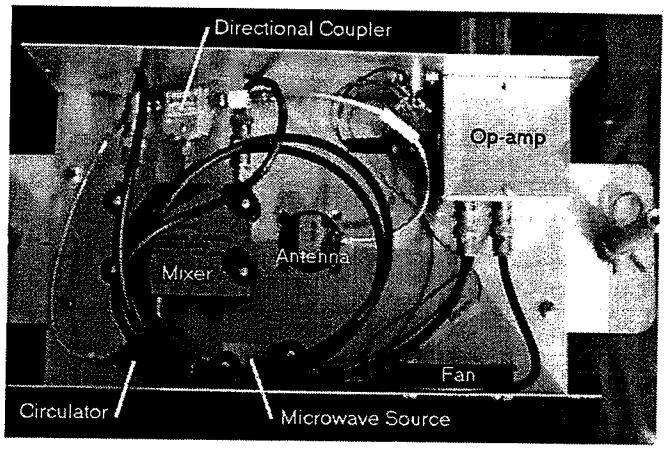

FIGURE 4.3 Internal Layout of Microwave Box

4.2.2.2 Supporting Structure

As described further in this section, the structure consists of both the microwave carts and the supporting arms. The microwave carts are made out of a wooden structure because it simplifies fabrication and has satisfactory vibration dampening properties compared to metal. The cart is comprised of two square frames, which are referred to as platforms, isolated from each other as shown in Figures 4.4 and 4.5. The lower platform is connected to the wheels and the supporting arms to the roller. A vibration dampening system is used to isolate any vibration between the upper platform and the lower platform. The upper platform carries the microwave equipment and the antenna.

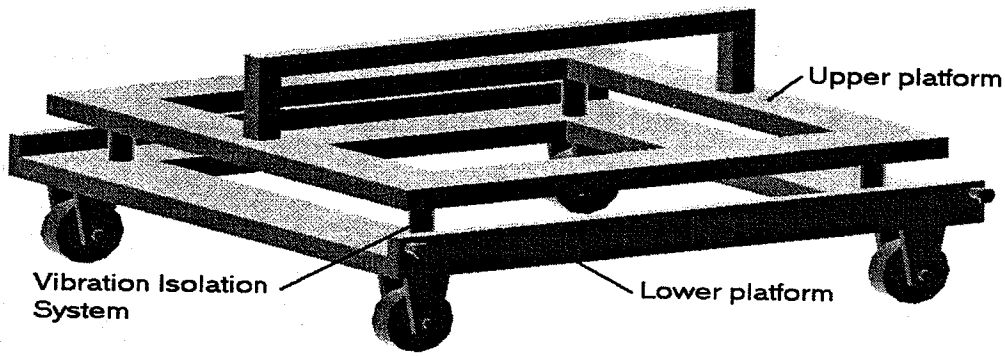

FIGURE 4.4 Preliminary Design of Microwave Cart

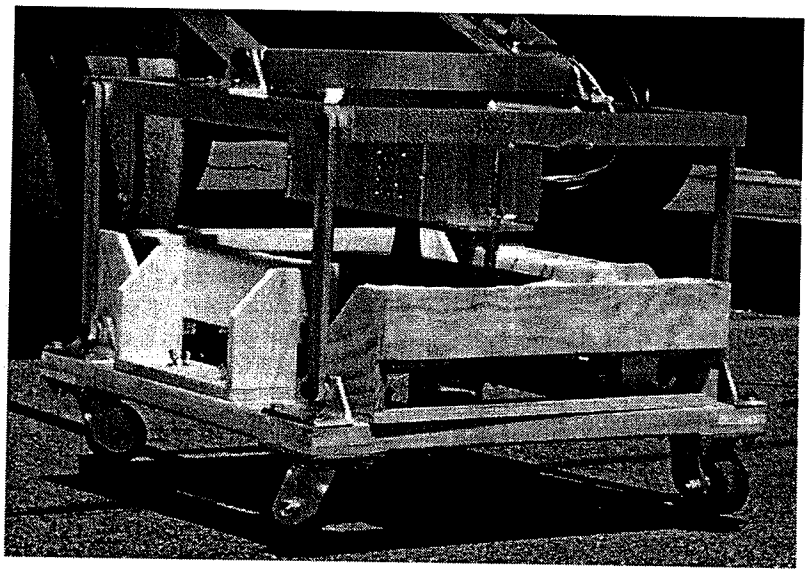

FIGURE 4.5 Completed Microwave Cart

The arms connecting the microwave carts to the vibratory roller are load-bearing structures. The arms are designed to carry the full weight of the microwave carts to prevent the carts from sinking into the tender hot asphalt pavement and rutting the surface. The arms also provide pivot points for the carts to swivel, allowing for changing surface elevations. Furthermore, the structure is shock mounted to reduce the vibration transmission to the carts. The photograph in Figure 4.6 shows one arm attached to the roller.

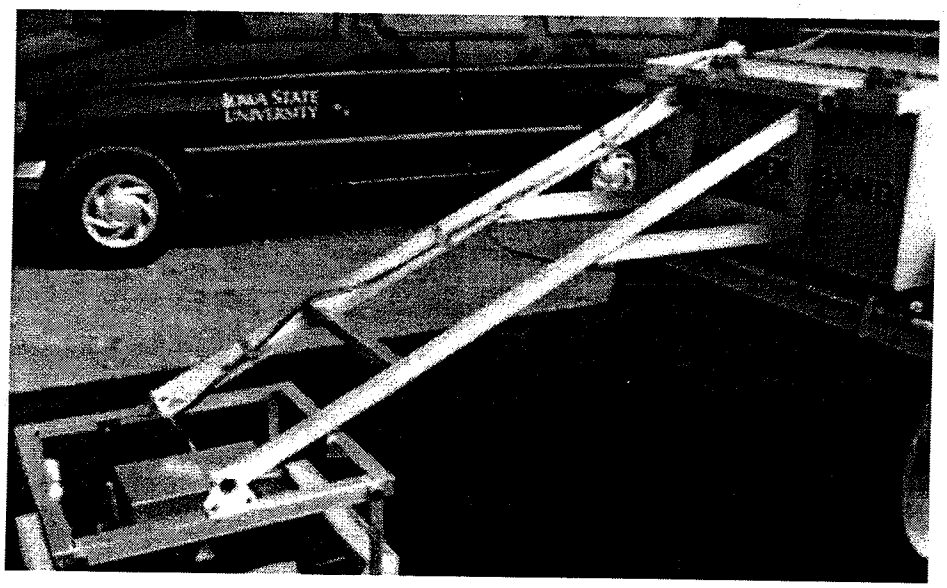

FIGURE 4.6 Support Arm

4.2.2.3 Vibration Dampening System

As discussed earlier, two types of vibration had to be considered. For the vibration transmitted from the vibratory roller through the structure, rubber isolation pads were used at each mounting point. Additionally, pivoting joints at the connecting locations of the supporting arms also allow for vibration isolation from the roller.

The second part of the vibration dampening system required more effort to develop. A mass-spring dampening system was chosen to isolate the upper platform of the microwave cart from all sources of vibration. This included transmitted vibration from the roller as well as ground vibration. A schematic of the system is shown in Figure 4.7. The springs are used to allow the upper platform to freely suspend from the lower platform. Dashpots, or airpots, are then used to absorb and dissipate the energy from the vibration. A dashpot uses an air chamber to dampen vibration with an adjustable dampening rate. The total weight of the upper platform had to be estimated to arrive at a suitable spring coefficient and a dashpot with a suitable dampening rate. Using Matlab, computer code was written to simulate the vibration dampening system with different spring coefficients and dashpot dampening rates.

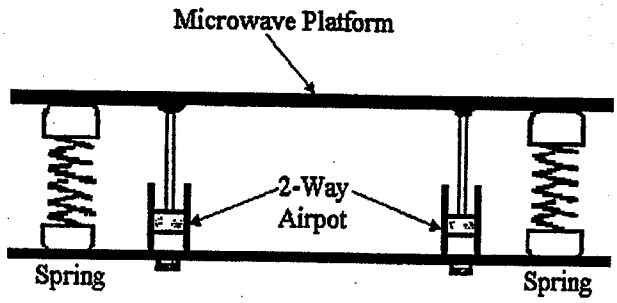

FIGURE 4.7 Mass Spring Dampening System

The major components of the vibration dampening system are the springs and the dashpots. Based on the vibration dampening simulation obtained using Matlab, a spring with spring constant of 5 lb/in was chosen. The weight of the upper platform and the microwave box were also factors in determining a suitable spring constant.

The dashpots were manufactured by Airpot Corporation based in Connecticut. The dashpots are fully adjustable units with a dampening rate of 0 to 30 in/s/s. The dashpots allow for vibration dampening in both tension and compression. Figure 4.8 shows the completed mass spring dampening system consisting of four springs and dashpots installed on a microwave cart.

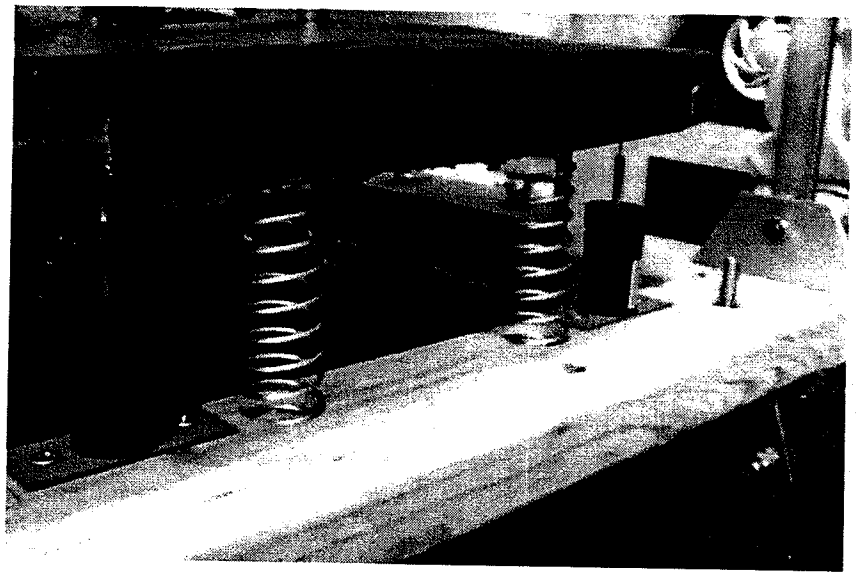

FIGURE 4.8 Spring and Dashpot System Mounted on Cart

4.2.2.4 Signal Sampling Regulator

A signal sampling regulator is required for the computer to take readings at regular intervals. The interval specified for the prototype is 2 cm. Taking readings at such intervals provided sufficient data points for an accurate reading and also not be too close to experience correlation between samples. This problem was approached by incorporating a third wheel to measure the precise speed of the vibratory roller. The speed measurement is then downloaded to the computer. The computer calculates the time interval to take measurements so that it corresponds to a measurement every 2 cm. The third wheel uses the theory of magnetic density. A magnetic target is mounted on the wheel, and every time it passes the magnetic sensor, a signal is sent to the computer. Based on the circumference of the wheel and the relationship with the roller drum, the speed of the roller can be calculated. The third wheel is attached to the roller on the rear drum. A schematic sampling regulator is shown in Figure 4.9.

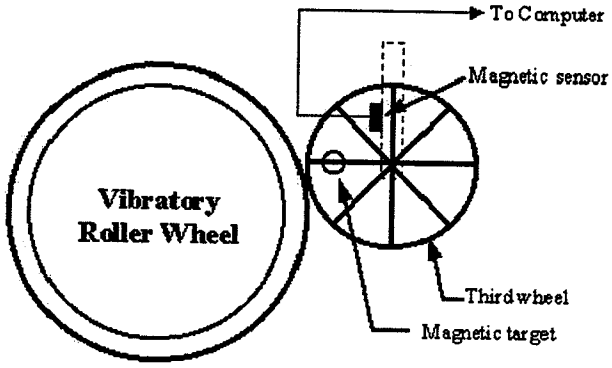

FIGURE 4.9 Signal Sampling Regulator Schematic

A bicycle fork and wheel were actually used to construct the main components of the signal sampling regulator. A round metal plate with eight equally spaced holes served as the target for the magnetic flux density device. The plate was attached to the wheel, and a sensor was attached to the fork. The sensor produces a constant 5-volt signal when it detects the metal plate. However, when a target is spotted, no voltage is produced and this is recognized by the computer. The speed of the roller can then be measured and the computer calculates the time interval to take the readings at 2-cm intervals. The mounted signal sampling regulator is shown in Figure 4.10.

4.2.2.5 Surface Water Removal System

The preliminary design of the prototype included a surface water removal system attached to the vibratory roller. This system used an air compressor mounted on the roller to pneumatically disperse surface water in the direct path of the microwave carts. Air nozzles were placed on the carts to blow away water in its path. A preliminary field test found that the required pressure for such a system to work was 100 psi. The test was performed on a parking lot that was being paved with hot mix asphalt. An air compressor with a variety of nozzle shapes and attachments was used for the test. Water was poured on the surface and dispersed using the different attachments at various pressures. An attachment with a line of ten 1/16 inch diameter holes operating at 100 psi was found to disperse water most effectively without damaging the soft asphalt surface.

The principal investigators decided that mounting a surface water removal system on the prototype was not critical in proving the validity of the differential concept. Furthermore, the water removal system posed many design complications in prototype development. First, an air compressor would have been required on the roller. This proved to be a problem with the limited amount of space on the small vibratory roller. The second concern was that an air compressor that would fit on the roller would not be able to continuously maintain the required pressure of 100 psi. The third issue was finding a power supply for the air compressor. In short, no air compressor currently on the market fit the requirements of this project.

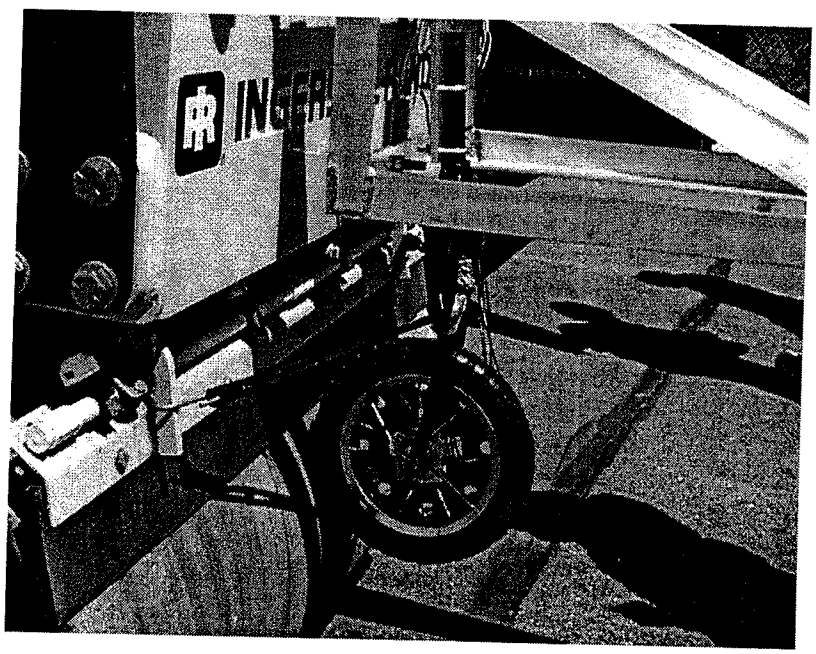

FIGURE 4.10 Sampling Regulator Mounted on Roller

A more feasible solution was devised. For the field tests, surface water would be removed manually. A person would follow the roller with a compressed air gun and simply disperse the surface water where necessary. Of course, this method is only feasible in the testing phases. A five-foot-long metal tube was fabricated as an attachment to the compressed air gun to keep a safe distance from the roller and yet be able to effectively remove surface water.

4.2.2.6 Completed Prototype

Figures 4.11 and 4.12 show the completed prototype.

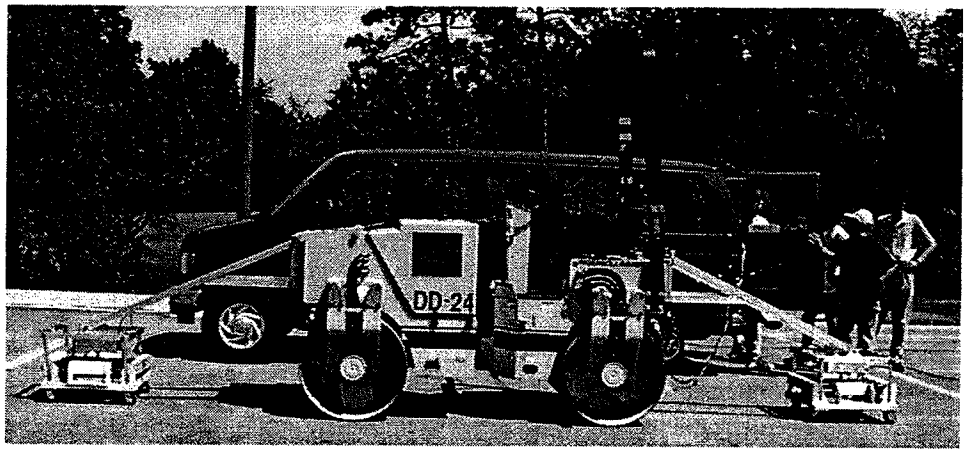

FIGURE 4.11 Side View of Prototype

FIGURE 4.12 Front View of Prototype

The prototype was designed so the computer including the A/D board could be placed in the van. A cable connected the microwave equipment on the carts and regulator mounted on the roller drum to the computer located in a van. Due to potential difficulties with vibration and ambient temperature potentially overheating the computer, the principal investigators decided against mounting all equipment on the roller. During the hot tests, the van drove alongside the roller, going forwards and backwards.

5.0 PROTOTYPE FIELD INVESTIGATION AND RESULTS

This chapter describes the procedure used to test the prototype MADS as well as the results. Two field tests involving hot mix asphalt (HMA) pavement were conducted (referred to as "hot" test). After the first hot test, some concerns had to be corrected on the prototype. After these issues were solved, a subsequent hot test followed. The second field test involving HMA generated some minor concerns as well. Results from these tests were inconclusive since the decreasing variance trend discovered during the preliminary field tests could not be replicated. It appears that additional technical issues with the prototype need to be resolved and further tests conducted before this idea can be validated. A more detailed discussion of the prototype testing phase and the results follows.

5.1 Prototype Field Investigation

Two field tests were conducted involving HMA. Both tests were conducted in Ames, IA, on property owned by Manatt's Inc., a local paving material supplier and contractor. Each test involved the use of one asphalt strip measuring 8 feet x 125 feet x 3 inches. The width (8 feet) of the mat allowed the research team to perform the test twice because there are four-foot-wide drums on an Ingersoll-Rand DD-24 roller.

Eight different densities were obtained in the first field test; while twelve were produced in the second test. The rolling pattern for both tests is shown in Figure 5.1. Notice that each section of a different density measures 70 inches long, corresponding to the distance between the centers of each drum. For each hot test, the roller continued compacting the mat even after optimal compaction had been reached to investigate signal properties on overcompacted asphalt pavement. In discussions with the manufacturer's representative, approximately eight passes were sufficient to achieve overcompaction using this particular vibratory compactor. Core samples were also taken to relate the variance of the signals to the densities. Figure 5.2 is a photograph of the site prior to laying the asphalt pavement for the second hot test.

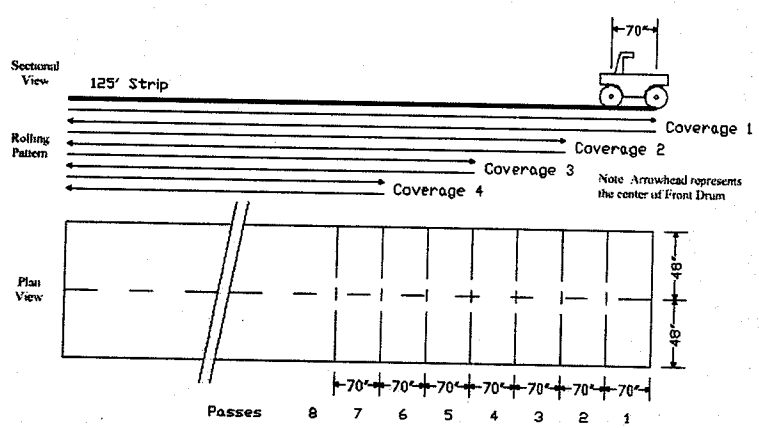

FIGURE 5.1 Hot Test Rolling Pattern

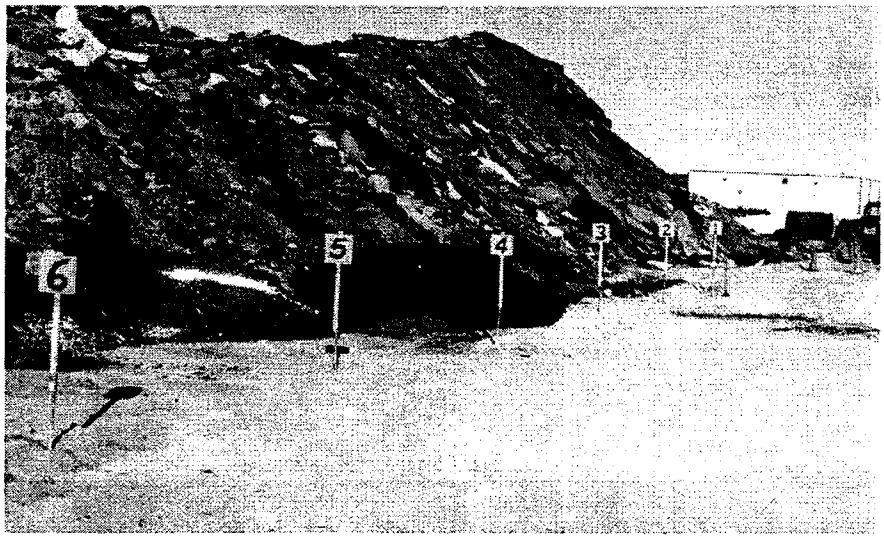

FIGURE 5.2 Photograph of Site Ready for Asphalt Pavement

In the first hot test, surface moisture was manually removed using an air compressor with a blowgun attachment. This approach worked only marginally well because the research team had difficulty keeping the air compressor running. In the second hot test, they decided to abandon the air compressor and have the operator spray a minimum amount of water on the drum to prevent sticking. Spraying small amounts of water on the drum worked quite well.

Both field tests experienced some technical difficulties. In the first test, the sampling regulator was taking samples every 8 cm instead of every 2 cm because of a problem with the A/D board in the computer. The research team also experienced difficulties with computer overheating, which were resolved by placing the computer in the van. In the second hot test, the microwave equipment worked properly, but the wheels on the carts got stuck in the asphalt pavement due to a slight slope on the test strip and a tender mix design (high percentage of fine aggregates and binder). In both hot tests, the first half of the strip was not usable. Therefore, the team was only able to take readings on the second half of each strip, which resulted in compacting a less-than-optimal mat with surface temperatures below 200°F during rolling. Figure 5.3, a photograph from the second hot test, shows the MADS in operation. Notice the cable extending from the microwave equipment on the roller to the van that is travelling parallel to the roller.

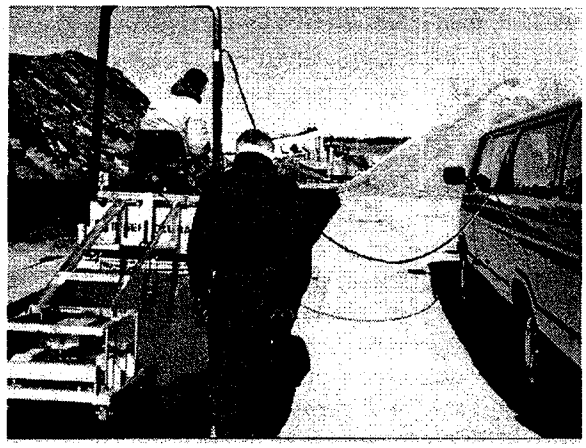

FIGURE 5.3 MADS in Operations

Microwave data consisting of both real and imaginary components were continuously collected for both the front and rear carts during the compaction process, allowing the research team to postprocess the data in a laboratory environment. Furthermore, a real-time data processing feature was also included in the software to continuously compute a 40-point moving average comparing the microwave signal in the front and back of the roller.

To correlate microwave signal variance to the in-place density, it was necessary to take core samples. Generally, two cores were taken from each density and then their values were averaged. Additionally, mix was sampled prior to the compaction process, and both the Rice and Marshall densities were determined. The team noticed that the mix designs for each field test were different. The mix design used during the second test included a higher percentage of fines

compared to the mix design in the first test, making the asphalt pavement softer and more susceptible to adhering to the cart wheels. Table 5.1 summarizes the mix design characteristics for each of the field tests, and Table 5.2 summarizes the core samples as percentages of the Rice and Marshall densities.

TABLE 5.1 Mix Design Characteristics

Asphalt Properties	First Field Test	Second Field Test
Mix type (per Iowa DOT)	A	B
Rice density (lbs./cu. ft.)	153.3	155.3
Marshall density (lbs./cu. ft.)	150.4	145.5

TABLE 5.2 Core Sample Densities

	First Field Test		Second Field Test	
Number of Coverages	% Rice	% Marshall	% Rice	% Marshall
1	89.5	91.2	85.0	90.7
2	91.1	92.9	86.0	91.7
3	92.3	94.1	87.6	93.4
4	93.4	95.2	88.0	93.8
5	93.8	95.6	88.8	94.8
6	94.2	96.0	89.4	95.3
7	94.8	96.6	90.0	95.9
8	94.8	96.6	90.4	96.4
9			89.8	95.8
10			89.8	95.8
11			91.2	97.3
12			90.7	96.8

Notice that after the eighth coverage during the second field test, the percentage of Rice density appears rather erratic. It decreased from 90.4 to 89.8, then increased to 91.2 on the eleventh coverage, and dropped slightly again on the twelfth coverage. This variance may result from uneven mat thickness, i.e., the core sample thickness varied from 3.33 inches to 4.72 inches, which led to different cooling and compaction rates. In the first field test, there was less thickness variability.

5.2 Data Analysis

Data analysis involved several steps: data extraction, pre-processing for large-scale variations and different sampling rates, and normality testing. The first step in analyzing the data involved extracting the useful data from the measurements taken. First, since the carts extend out significantly in front and behind the roller, the first measurements from the trailing cart are not on properly compacted asphalt. The same is true for the last measurements of the leading cart. This extra data at the beginning and end are discarded such that the measurements from the two carts are from the same location. Finally, the data near the stopping point of the roller is discarded from the first pass, since this area of the pavement is not included in the final pass measurements [1].

Pre-processing was necessary since it was found that the data had significant variation from one area of the pavement to another. These large-scale variations affect the resulting variance, especially in the field prototype tests where a longer section of pavement was used (compared to the preliminary field tests). In order to remove these variations (which are most likely not due to the pavement density) a high pass filter was used. A scale-length of 200 cm was arbitrarily selected as larger than the variations that appear to be caused by density, and smaller than the problematic large-scale variations. The filtering process used a 4th order Butterworth high-pass filter on the complex reflection coefficient [1]. Figure 5.4 shows a section of the real and imaginary components of the data before and after filtering.

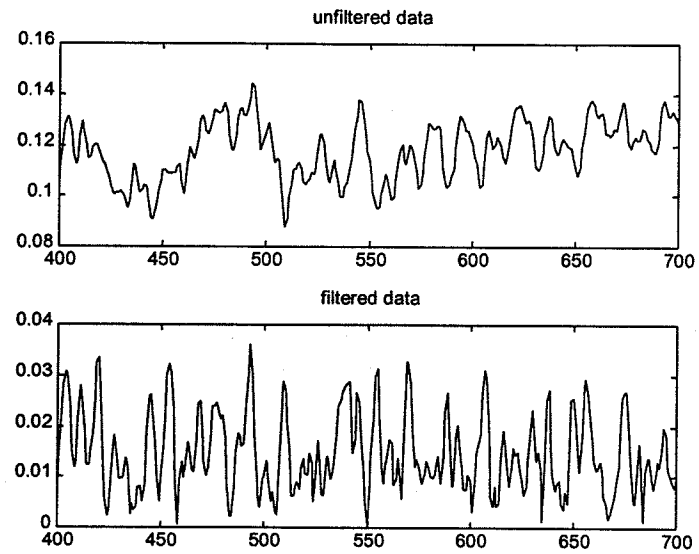

FIGURE 5.4 Before and After Results from Filtering Large-scale Variations

In addition to filtering the data, the differing sample rates had to be considered. In the preliminary field tests, samples were taken every 2 cm, while in the first prototype field test, samples were taken every 8 cm due to a software error. In the second prototype field test, samples were taken every 1cm. In order for the confidence analyses to be accurate, the samples themselves are required to be independent of each other. Extensive auto correlation analysis revealed that samples taken every 1 cm are highly correlated while samples taken every 2-3 cm are not correlated [1].

The Kolmogoroff-Smirnoff (K-S) test was performed on the prototype field data to be sure the distribution assumption is valid for this data also. The test was performed twice, first on the unfiltered data, and again on the filtered data. As can be seen in Figure 5.5, the data appear to fit the Rayleigh distribution quite well; this is, in fact, a better fit than the preliminary field data. This better looking fit is primarily caused by the increase in the number of data points, which is taken into consideration in the K-S test. However, the K-S test results show that much of the data themselves are a better fit as well [1].

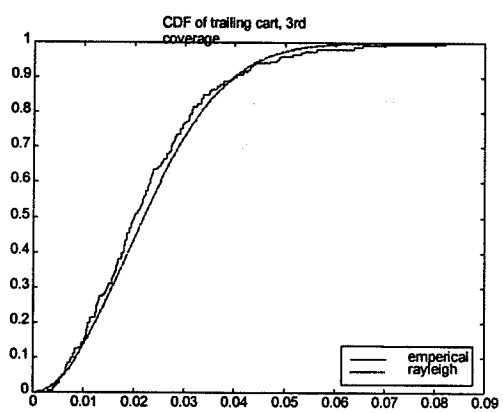

FIGURE 5.5 Example Cumulative Distribution Frequency (CDF) from First Prototype Field Test

All of the new data from both of the new tests pass the K-S test at significance levels well above 0.2. The one concern involves the data from the front cart in the second prototype field test. There are many data points from this cart that were discarded in the K-S test procedure. One explanation for this is that the front cart had the most problems on the first half of the strip. During the test it was noticed that this cart was bouncing more than normal due to the asphalt buildup on its wheels from being stuck in the soft asphalt earlier [1].

5.3 Prototype Results

Despite the fact that the microwave components were calibrated to produce identical readings, and the carts were both built of the same design, resulting variances differed between the two carts. In addition, the variance results were different depending on which direction the cart was travelling. These differences made analysis of the results more complicated. Unfortunately, each cart only sees half of the densities of the pavement, so separating the results would not give a very good overall picture. To obtain this picture, the data sets from the two carts had to be combined. Since the results differed from the same cart depending on if it was leading or trailing, two graphs are shown one with the leading data and one with the trailing cart data. In order to combine the results from the two different carts, the variances had to be normalized. The method used for this normalization was to multiply a constant to one of the cart's variances such that the variances between 93-95% Rice density exhibited a downward trend in this range. Figure 5.6 shows the leading and trailing results versus coverage from the first field prototype test. It can be seen that while most of the data follows the trend previously found, coverages 5 and 6 in particular do not agree between the leading and trailing data. While the leading cart is taking data from the fifth coverage, the trailing cart is taking data from the sixth coverage; therefore, the two high points shown here are actually from data taken simultaneously. It is possible something went wrong while taking these data. Figure 5.7 shows the densities measured corresponding to these coverages [1].

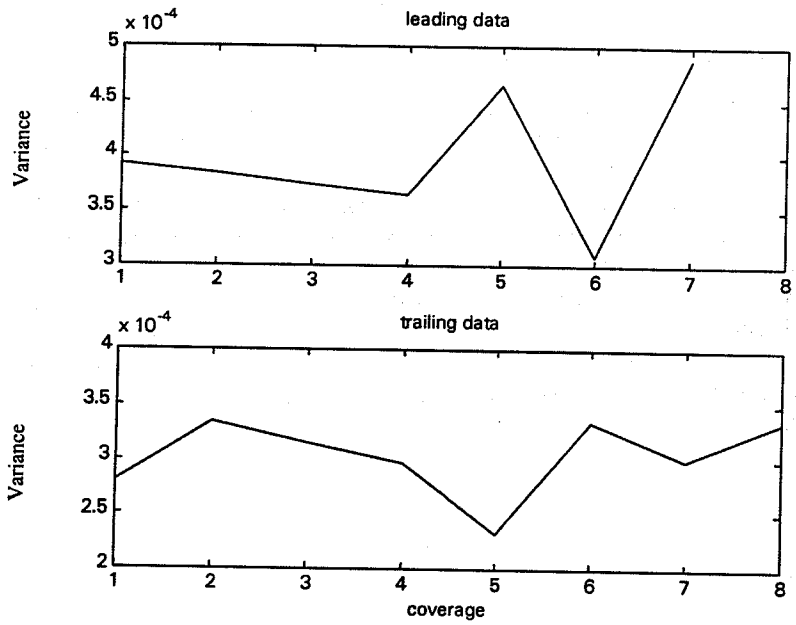

FIGURE 5.6 First Test Results versus Coverage

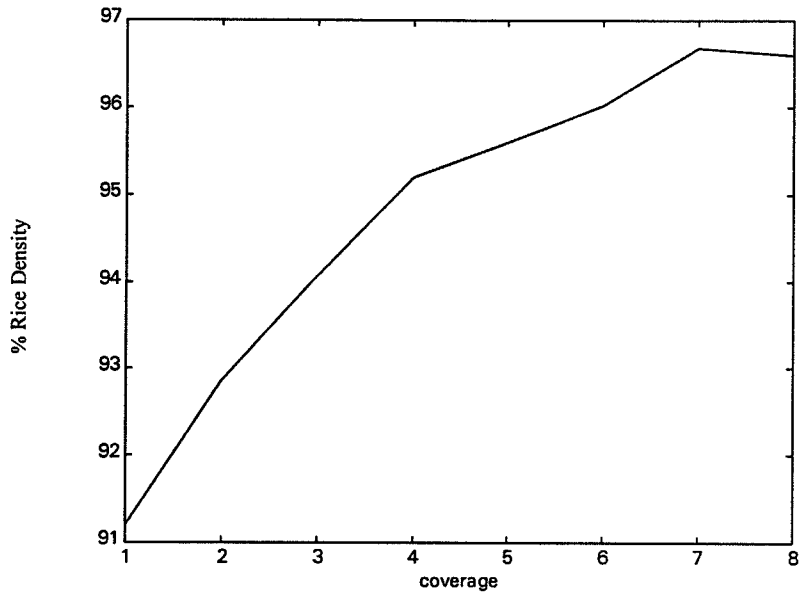

FIGURE 5.7 Density versus Coverage for First Field Prototype Test

The second field prototype test results are shown in Figures 5.8 and 5.9. This experiment continued well into the over compaction range; however, the results from the beginning of this test also exhibit a similar trend to the other experimental results. This time the leading and trailing data agree except in the trailing data where the increase begins at coverage 5 instead of 6. As mentioned in the previous chapter, the actual density measurements in this experiment are suspect, so it is difficult to know if this increase corresponds to the 95%-96% Marshall density measured or if it might actually be a higher density as found in the preliminary field tests. This density measurement problem becomes obvious in the fluctuation in density for the 8th though 12th coverages. In addition, the maximum density measured is only 97% of the density achieved in the lab with the same mix. Plotting these results directly against pavement density would not make sense, so separate variance and density results are shown versus coverage [1].

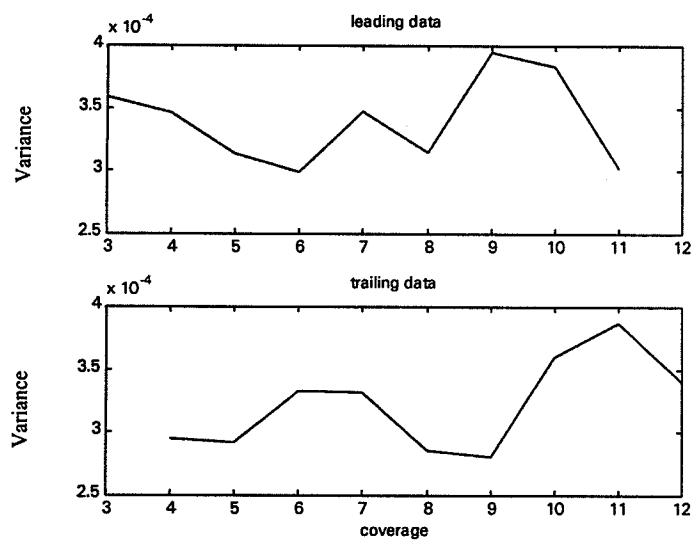

FIGURE 5.8 Second Field Prototype Test versus Coverage

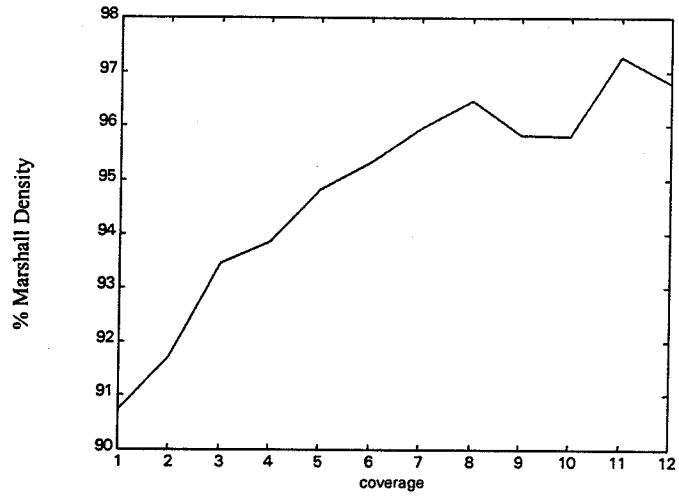

FIGURE 5.9 Density versus Coverage for Second Field Prototype Test

Figure 5.10 shows the 80% confidence intervals on the individual cart results from the first field prototype test, and Figure 5.11 shows the confidence intervals for the second field prototype test. While the confidence has been increased by the increased number of measurements, these new experiments do not show the same magnitude of variance change from one coverage to another. Therefore, the variations of these two field tests are mostly within the error bounds.

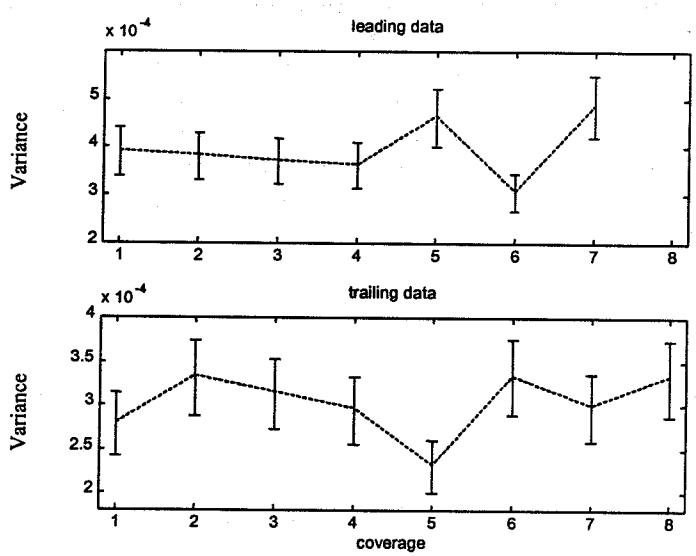

FIGURE 5.10 Confidence Intervals on First Field Prototype Test Results

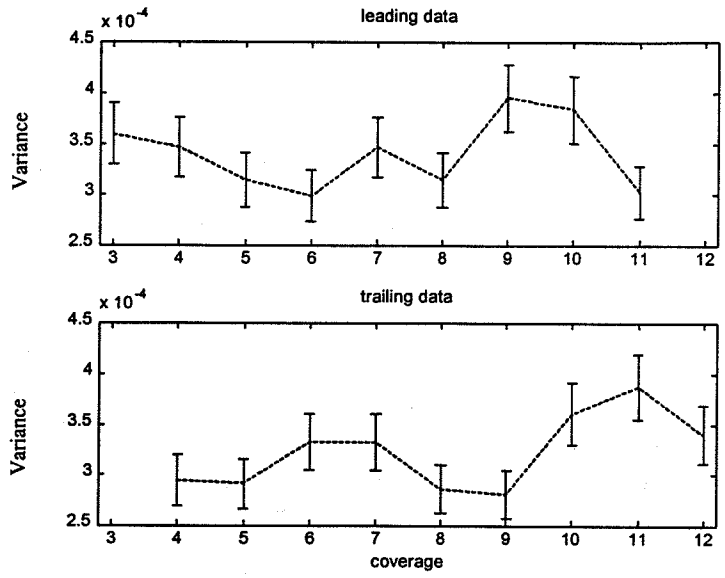

FIGURE 5.11 Confidence Intervals on Second Field Prototype Test Results

As an experiment to determine the interaction of the subbase, two aluminum plates measuring 12 inches by 12 inches were placed on the subbase and paved over with asphalt to determine if the microwaves penetrated into the subbase. Data processing revealed that the microwaves did not significantly penetrate the subbase. The data showed no obvious difference when the carts passed over the area where the plates were placed. This finding should be investigated further because it did not confirm the laboratory results provided by VU. Their results showed that at 8.5 GHz, some subbase penetration should be anticipated.

5.4 Results Summary

Based on the results from the two field prototype tests, it is evident that additional experimentation is required before one can clearly establish the viability of this idea. Despite the significant amount of effort expended by the research team to design, build, and test the first microwave asphalt pavement sensor, it appears that there still may be additional technical issues to be resolved. These tests provided the team with valuable insights into how to better design this innovative sensor for the next phase.

6.0 CONCLUSIONS

6.1 SUMMARY

During this NCHRP IDEA project, the research team investigated the use of microwaves to determine asphalt pavement density during the compaction process. Field investigations prior to the project's start revealed that variance in the return signal decreased as density increased. At approximately 93% of the Rice density, signal variability significantly increased followed by further decreases in signal variance. On the basis of these findings, the research team thought that the idea showed merit and deserved further exploration.

This project involved (1) developing a better understanding of the electrodynamical relations between microwaves and asphalt pavement; (2) designing, building, and testing a prototype; and (3) summarizing the results. Vilnius University performed extensive laboratory tests on several small samples containing two types of aggregate and binder, discovering several important relationships. Iowa State University performed laboratory tests on large samples and found a similar variance trend in the preliminary field tests. A microwave asphalt density sensor (MADS) was designed and constructed, using findings from the laboratory experiments and the preliminary field tests. Two field tests involving the MADS were conducted. The research team experienced difficulties during both field tests that compromised some of the results (e.g., hardware and software issues and cart wheels that "stuck" in the asphalt). Results from these tests were inconclusive since the decreasing variance trend discovered during the preliminary field tests could not be replicated. It appears that additional technical issues with the prototype need to be resolved and further tests conducted before this idea can be validated. In the next section, recommendations for enhancing the MADS approach are provided.

6.2 RECOMMENDATIONS

Several recommendations are provided to further explore the viability of this idea. The research team strongly recommends modifying the carts and supporting arm structures to prevent the cart wheels from "sticking" in the pavement, a particular concern during the second field test. Perhaps an even better approach would involve eliminating the carts and supporting the antennas in a cantilever fashion in the front and back of the roller. For increased protection, one of the antennas could even be mounted in the middle of the roller.

Another solution would be to eliminate the carts completely and use only one antenna mounted in the center of the roller. The differential approach can still work with one antenna as long as the roller operator compares signal variance from one coverage to another. As long as there is a decreasing variance trend, the operator would continue compacting that particular zone before moving to another part of the mat.

The microwave frequency may also need to be investigated and perhaps increased. It is not clear how strong an effect the subbase has on the return signal. The team recommends that this issue be further investigated in the next phase.

It would also be advantageous to conduct further field tests involving different mix designs, because this affects the point at which an increase in variance is sensed. Additional research is required to identify which mix designs should be considered.

Furthermore, the sensor should be tried on a larger breakdown roller that might only make four to five coverages. Finally, future work on the sensor should involve a microwave technology company that is interested in supporting such a product.

6.3 CONCLUSIONS

As this project demonstrated, there are several opportunities for enhancing the microwave asphalt pavement sensor. Due to technical difficulties experienced during the two prototype field tests, it is too early to judge the viability of this concept. Preliminary field tests have shown that a relationship exists between the variance of the reflected microwave signals and the density of an asphalt pavement. Another step has been taken to use this relationship (using a differential approach) to measure the compaction level of asphalt pavements during the compaction process, giving a real-time indication of in-place density. Much knowledge was gained from this research project, and on the basis of these findings, further testing and refinement of the prototype is recommended to produce the expected results. This innovative microwave asphalt density sensor would make an important contribution to the construction industry if it is proven to work satisfactorily in the field environment.

ACKNOWLEDGEMENTS

The principal investigators and co-investigators thank several people for their involvement with this project. The project's success can be directly attributed to their support, advice, and encouragement. We extend special thanks to Dr. K.T. Thirumalai and Dr. Inam Jawed at the NCHRP-IDEA program for their financial support of, helpful advice on, and interest in this project. Additionally, we extend our appreciation to our advisory panel consisting of the following members:

John Heggen/Todd Hansen (Substitute), Iowa Department of Transportation
Kim Bentley, Center for Advanced Technology and Development, Iowa State University
Donald Jordison, Asphalt Paving Association of Iowa
Dr. Dah Yinn Lee, Iowa State University
Tom Manatt, Manatts, Inc.
Mani Mina, New Technology Resource Group
Francisco Romero, Geophysical Survey Systems, Inc.
Peter Sawchuk, TransTech Systems, Inc.
Dale Starry, Ingersoll-Rand
Randy Web, Blaw-Knox

Special thanks go to the Iowa Department of Transportation for their support in preparing asphalt pavement samples for the laboratory testing at Iowa State University. In particular, we recognize John Heggen, Dan Seward, and John Hinrichsen for assisting in the sample preparation.

The Center for Advanced Technology and Development provided financial support and guidance for the preliminary field studies. We sincerely thank both Kim Bentley and Karen Jenkins (former employee) for their assistance.

Moreover, Dr. Dah Yinn Lee was instrumental during the early planning and laboratory analysis phases. His support, guidance, and encouragement were much appreciated.

Peter Sawchuk provided invaluable guidance in terms of marketing the sensor.

Much appreciation is also due to Dale Starry for allowing the research team to use an Ingersoll-Rand DD-24 roller for this project. Additionally, his comments and help during the second field test were much appreciated.

Several students at Iowa State University were also involved in the prototype development and testing phase of this project. Special thanks are extended to the following students: Lay Yee Lim, Daniel Fahrion, Stephen Fung, Hyun Ho Park, Lawrence Tan, Nick VandeGriend, and S. Xiong. Without their devoted assistance, the prototype would not have been possible.

We also thank Ames Laboratory at Iowa State University for assisting in the design and fabrication of the support arms, carts, and signal sampling regulator.

REFERENCES

1. D. F. Fahrion. Confidence Intervals for Statistical Methods of Data Analysis, Master's Thesis, Iowa State University, Ames, May 1999.

2. H.C. Han, E. J. Jaselskis, S. Xiong, and D. Fahrion. Measurements of Asphalt Density Using Microwaves, to appear in Review of Progress in Quantitative Nondestructive Evaluation, Vol. 18, Plenum, New York, 1999.

3. L. Tan. Prototype Construction and Field Tests of the Microwave Asphalt Density Sensor, Master's Thesis, Iowa State University, Ames, December 1998.

APPENDIX A:

DIELECTRIC CYLINDER OF ANY SIZE RECTANGULAR WAVEGUIDE

To determine the dielectric parameters of the asphalt samples of different density in the microwave range, the complex reflection and transmission coefficients of the cylindrical dielectric rod placed in the rectangular waveguide were calculated taking into account the non-homogeneous distribution of the rod's microwave field. Consider a dielectric cylinder of complex permittivity, ε^*, and any radius, r_0, placed centrally ($l = 0$) in a guide so that the cylinder axis is parallel to the electric field vector of the dominant TE_{10} - mode (Figure A.1). Consider the most complicated case where the cylinder's microwave wavelength may be of any value, including the value of the same order as its dimensions. This was the situation for the small asphalt samples provided. This complicated case requires a rigorous solution using Maxwell's equations.

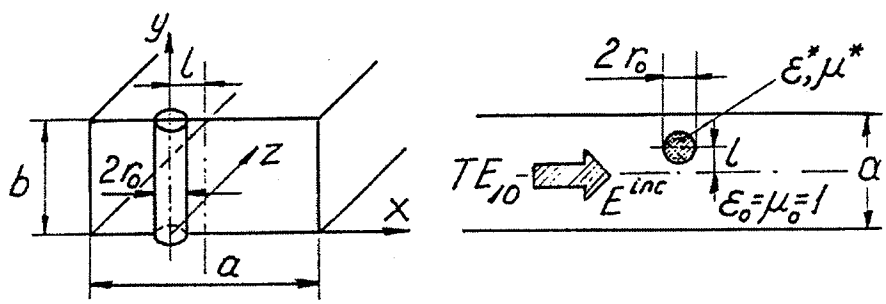

FIGURE A.1 Cylindrical Dielectric Rod in Rectangular Waveguide

The tangential components of the cylinder's electric and magnetic field can be expanded as a sum of the partial waves:

$$E_y^c \sim \sum_{m=-\infty}^{\infty} A_{1,m} J_m(\beta) e^{im\varphi},$$
$$H_\varphi^c \sim -i\left(\varepsilon^* \frac{\varepsilon_0}{\mu_0}\right)^{1/2} \sum_{m=-\infty}^{\infty} A_{1,m} J'_m(\beta) e^{im\varphi}. \tag{1}$$

where J_m are Bessel functions, J'_m is the Bessel functions derivative, φ is the polar coordinate, $\beta = k(\varepsilon)^{1/2}r$, ε_0 and μ_0 are electric and magnetic permittivities of free space, respectively.

Similarly, the scattered field outside the cylinder is given by

$$E_y \sim \sum_{m=-\infty}^{\infty} A_{2,m} H_m^{(2)}(\alpha) e^{im\varphi},$$

where $A_{1,m}$ and $A_{2,m}$ are the complex expansion coefficients, $H_m^{(2)}$ is the Hankel function of the second order, $\alpha = kr$.

A set of complex linear equations for the determination of the unknown complex coefficients is found by applying the boundary conditions at the cylinder's surface $r=r_0$. They may be recast in the form

$$\sum_{m=-\infty}^{\infty} S_{m,n} A_{2,n} - X_m A_{2,n} = A_{0,m'}, \tag{2}$$

where

$$X_m = \frac{(\varepsilon^*)^{1/2} H_m^{(2)}(\alpha_0) J'_m(\beta_0) - H_m^{(2)'}(\alpha_0) J_m(\beta_0)}{(\varepsilon^*)^{1/2} J_m(\alpha_0) J'_m(\beta_0) - J'_m(\alpha_0) J_m(\beta_0)} \tag{3}$$

$$S_{m,n} = (-1)^{m+n}\left(S_{1,n+m} - S_{3,n-m}\right) + S_{2,n+m} - S_{3,n-m},$$
$$A_{0,m} = -\frac{1}{2}\left[i^m e^{i(m\varphi_1 - k_x l)} + (-i)^m e^{-i(m\varphi_1 - k_x l)}\right],$$
$$k_x = \frac{\pi}{a}, \quad \cos\phi_1 = \frac{\pi}{k_0 a},$$

and the coefficients S_1, S_2 and S_3 involve the images of the cylinder with respect to the narrow waveguide walls and are given by

$$S_{1,n+m} = \sum_{p=0}^{\infty} H_{n+m}^{(2)}\left\{k_0\left[(2p+1)a + 2d\right]\right\},$$
$$S_{2,n+m} = \sum_{p=0}^{\infty} H_{n+m}^{(2)}\left\{k_0\left[(2p+1)a - 2d\right]\right\}, \tag{4}$$
$$S_{3,n-m} = \sum_{p=1}^{\infty} H_{n-m}^{(2)}\left(2k_0 ap\right).$$

The coefficients $A_{1,m}$ are expressed as follows:

$$A_{1,m} = \frac{J_m\left[A_{0,m} - \sum_{n=-\infty}^{\infty} S_{n,m} A_{2,n}\right] + H_m(\alpha_0) A_{2,m}}{(\varepsilon^*)^{1/2} J_m(\beta_0)}. \tag{5}$$

As previously described, the amplitude reflection and transmission coefficients are obtained by determining the electric and magnetic field inside the cylinder. They can be written as follows:

$$R^* = C^*\left(-TE_{10}\right), \quad T^* = 1 + C^*\left(+TE_{10}\right), \tag{6}$$

where

$$C^*\left(\pm TE_{10}\right) = \frac{i(\varepsilon^* - 1)}{2y} I_{\pm},$$
$$I_- = -\frac{4\pi k_0}{a(\varepsilon^* - 1)}\beta_0 \sum_{m=-\infty}^{\infty} (-1)^m A_{1,m} A_{0,m}\left[(\varepsilon^*)^{1/2} J_{m+1}(\beta_0) j_m(\alpha_0) - J_m(\beta_0) J_{m+1}(\alpha_0)\right], \tag{7}$$
$$I_+ = I_-\Big|A_{0,-m} \to A_{0,m}^-, \quad A_{0,m}^- = A_{0,m}\Big|\varphi_1 \to -\varphi_1.$$

For a finite number of terms in the summation, the system (Equation 2) can be solved using a computer. Note that when the cylinder's radius decreases, the contribution of the higher waves becomes negligible and the zero term ensures sufficient accuracy. This case is the most interesting for all practical purposes as it involves dielectric spectroscopy of ferroelectrics and related materials.

The derived equations (7) have no limitations in regards to the cylinder's radius and the permittivity.

In the general case, the number of waveguide modes, which should be taken into account by solving Equations 1 and 2, depends on the cylinder's radius. A computer program, considering only even terms m=0, ±2, ±4, ±6, ±8, ±10, showed satisfactory agreement between computational and experimental results obtained, using p-germanium samples of known permittivity (ε = 12.8) up to the complete filling of the cross section of the waveguide ($kr_0 \cong 2.1$) with the cylindrical samples. At a definite kr_0, a resonant transmission occurs and a lossless cylinder acts as a matched load in a guide. The results showed that the cylinder's electric field, in general, is highly non-homogeneous.

APPENDIX B:
DETERMINATION OF DIELECTRIC PARAMETERS

In the centimeter wave range, the complex reflection and transmission coefficients of the TE_{10} – wave, produced by a nonmagnetic sample in a rectangular waveguide whose sample axis is parallel to the electric field vector, are defined by (1) a complex dielectric permittivity (or complex conductivity); (2) the sample's dimensions; and (3) the frequency and width of a waveguide's wide wall, i.e., $R = f(\varepsilon^*, r, \nu, a)$. Using a computer, the dielectric parameters $\varepsilon^*(\nu, T)$ can be calculated by solving the nonlinear complex equations $\varepsilon^* = f(R, T)$ or $\varepsilon^* = f(R^*)$. The latter case provides a better convergence, but it leads to an indetermination, which arises when determining ε^* from the moduli R and T (for n = 0 only). In this case, the proper value of permittivity is chosen analytically.

The complex reflection coefficient $R^* = Re^{i\varphi}$ can be expressed as follows:

$$R = f_1(\varepsilon', \varepsilon''),$$
$$\varphi = \varphi_2(\varepsilon', \varepsilon''). \tag{1}$$

Having experimentally measured the values, R and φ, one can obtain a set of two nonlinear equations with respect to ε' and ε'', which can be solved using a computer.

Measurements of moduli of the reflection and transmission coefficients by network analyzers were more convenient experimentally, especially when sweeping a frequency. In this case, the research team obtained the set of two nonlinear equations with respect to the moduli of R* and T*:

$$R = f_1(\varepsilon', \varepsilon''),$$
$$T = f_2(\varepsilon', \varepsilon''). \tag{2}$$

Equations (4) and (5) found in Appendix A were solved by a modified Newton's method. Then, the set of nonlinear equations was transformed to the set of linear equations:

$$\varepsilon'_{n+1} = (ED_2 - FD_1) / (C_1D_1 - D_1C_2),$$
$$\varepsilon''_{n+1} = (FC_1 - EC_2) / (C_1D_1 - D_1C_2), \tag{3}$$

where

$$C_1 = [f_1(\varepsilon'_n, \varepsilon''_n) - f_1(\varepsilon'_{n-1}, \varepsilon''_n)] / [\varepsilon'_n - \varepsilon'_{n-1}],$$
$$D_1 = [f_1(\varepsilon'_n, \varepsilon''_n) - f_1(\varepsilon'_n, \varepsilon''_{n-1})] / [\varepsilon''_n - \varepsilon''_{n-1}],$$
$$C_2 = [f_2(\varepsilon'_n, \varepsilon''_n) - f_2(\varepsilon'_{n-1}, \varepsilon''_n)] / [\varepsilon'_n, - \varepsilon'_{n-1}],$$
$$D_2 = [f_2(\varepsilon'_n, \varepsilon''_n) - f_2(\varepsilon'_n, \varepsilon''_{n-1})] / [\varepsilon''_n - \varepsilon''_{n-1}],$$
$$E = R - f_1(\varepsilon'_n, \varepsilon''_n) + C_1\varepsilon'_n + D_1\varepsilon''_n,$$

Preliminary values of ε'_{min}, ε'_{max} and ε''_{min}, ε''_{max} were selected from measurements of the dielectric parameters of the asphalt samples at radio frequencies. The calculation stops when

$$R - f_1(\varepsilon', \varepsilon'') < \delta R, \tag{4}$$

and

$$T \text{ (or } \varphi) - f_2(\varepsilon', \varepsilon'') < \delta T \text{ (or } \delta\varphi).$$

One can select, for instance, $\delta R \leq 0.001$ and $\delta T \leq 0.001$, or $\delta\varphi \leq 0.1°$, and calculate with reasonable accuracy the dielectric parameters of the measured samples.

Figure B.1 shows the dielectric spectrometer setup for the measurements of the moduli of the reflection and transmission coefficients controlled by a computer. Using the backward-wave oscillators as variable frequency sources and changing only the waveguides terminating with the matched load, the 8 to 80 GHz frequency range can be covered. This setup was used to determine the dielectric parameters of the asphalt samples in the 8 to 12 GHz frequency range.

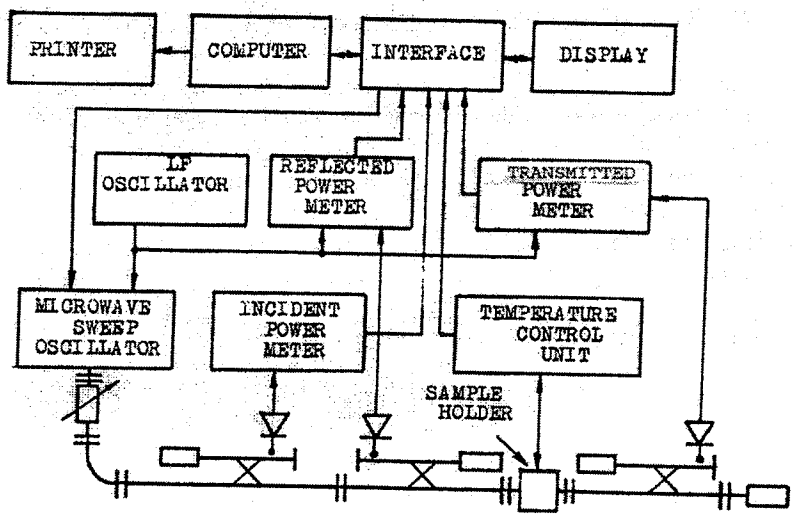

FIGURE B.1 Microwave Dielectric Spectrometer Setup for Measurements of Permittivity and Losses of Asphalt Samples

The spectrometer works as follows. The microwaves, generated by a sweep oscillator through the waveguide system and two couplers, travel to the sample holder with an asphalt sample placed in the waveguide as shown in Figure A.1. The incident power meter measures incident signals, and the reflected power meter measures the reflected part of the signal from the asphalt sample. The transmitted part of the incident signal measures the transmitted power meter. All three signals, via the interface, are relayed to the computer, which, using the above equations, calculates the dielectric parameters—permittivity and losses—of the asphalt samples. When the temperature control unit changes the temperature of the sample holder, the temperature dependencies of the measured parameters are obtained.